SEDIMENT DEPOSITION IN THE LOWER HUDSON RIVER ESTUARY

By
Jonathan Dalrymple Woodruff
B.S. Tufts University, 1996

Submitted in partial fulfillment of the requirements of the degree of

Master of Science in Civil and Environmental Engineering
at the
MASSACHUSETTS INSTITUTE OF TECHNOLOGY
and the
WOODS HOLE OCEANOGRAPHIC INSTITUTION

September 1999

Signature of Author _____

Joint Program in Civil and Environmental Engineering
Massachusetts Institute of Technology
Woods Hole Oceanographic Institution
September 1999

Certified by _____

Wayne R. Geyer,
Woods Hole Oceanographic Institution
Thesis Supervisor

Certified by _____

Heidi M. Nepf,
Massachusetts Institute of Technology
Thesis Reader

Accepted by _____

Michael S. Triantafyllou, Chair,
Joint Committee for Applied Ocean Physics and Engineering
Massachusetts Institute of Technology/Woods Hole Oceanographic Institution

Accepted by _____

Daniele Veneziano,
Chairman, Departmental Committee on Graduate Studies
Massachusetts Institute of Technology

Sediment Deposition In The Lower Hudson River Estuary

by

Jonathan Dalrymple Woodruff

Submitted to the Department of Civil and Environmental Engineering on August 6, 1999 in partial fulfillment of the requirements for the MIT/WHOI Joint Program degree of Masters of Science in Civil and Environmental Engineering

Abstract

This study uses geophysical and sedimentological data collected from the Lower Hudson River estuary to identify the depositional response of the estuary to high river discharge events. Erosional and depositional environments in the estuary are identified through the use of side-scan sonar, bottom penetrating sonar and surficial sediment sampling. Sediment cores are used to document deposit thicknesses and to obtain the spatial distribution of estuarine deposits.

Results show a high degree of spatial and temporal variability in sedimentation within the estuary. Two primary deposits are identified underneath the turbidity maximum for the estuary. Approximately 300,000 metric tons of sediment were deposited within these two deposits during May and June of 1998. This short-term accumulation underneath the turbidity maximum of the estuary can account for 30 to 98 percent of the estimated, river-borne sediment load supplied to the estuary during the 1997-1998 water year. Both the tidally produced stratigraphy observed in sediment cores and the spatial distribution of identified deposits, support the theory that sedimentation underneath the turbidity maximum of the estuary is primarily the results of a convergence in bottom water flow, caused by the formation of a salinity front during ebb tide.

Thesis Supervisor:
Dr. Wayne R. Geyer
Woods Hole Oceanographic Institution

Acknowledgments

This work would not have been possible without the generous support by the scientific and technical communities at both the Woods Hole Oceanographic Institution and the USGS Woods Hole Field Center. I am especially grateful to my advisor Dr. Rocky Geyer, whose knowledge and guidance have been invaluable in the production of this thesis. I would like to thank Dr. Neal Driscoll and Dr. Chris Sommerfield for their help in the collection and analysis of the geophysical and sedimentological data used in this study. I also appreciate the time spent by Dr. Heidi Nepf reading and commenting on this thesis. Finally, I would like to thank Julie for her patience and encouragement and my family for their support. My deepest gratitude to all of you. This research was funded by the Hudson River Foundation and a National Science Foundation Coastal Trainee Fellowship.

1 Introduction

The Hudson River estuary flows into one of the the world's most important seaports, carrying sediment that must be continuously dredged from New York Harbor [Panuzio, 1965, Gross, 1974]. The accumulation of contaminants within this sediment has dramatically increased the cost of dredging for the port and has threatened the many birds, fish and shellfish that use the estuary as feeding, nesting, breeding and spawning grounds [ACOE, 1996, Long et al., 1995, Squibb et al., 1991]. These effects increase the importance of understanding how sediment is transported and deposited within the estuary.

Dredging records indicate that approximately 2.2 million metric tons (dry weight) of sediment are deposited within New York Harbor annually [Gross, 1974]. Approximately 330,000 metric tons of this sediment inventory is deposited on the west side of the Hudson River estuary between km 10 and km 16 [1]. Sediment accumulation rates within this mid-estuarine deposit are between 5 and 70 cm/yr [Olsen et al., 1978, Olsen, 1979], two orders of magnitude larger than rates found on the deeper east side of the channel and one order of magnitude larger than accumulation rates found upstream.

Recent studies have identified that a turbidity maximum exists within the Lower Hudson River estuary whose location is consistent with this mid-estuarine deposition

[1] Positions along the Hudson River estuary are measured in kilometers northward along the river channel beginning at the Battery on the southern tip of Manhattan.

[Hirschberg and Bokuniewicz, 1991, Geyer, 1995, Geyer et al., 1997]. Peak near-bed suspended sediment concentrations during the tidal cycle range from 100-1000 mg/l with in this region, much larger than the 20-40 mg/l observed for most of the estuary.

Turbidity maxima are frequently observed within estuaries. This phenomenon has been explained by a number of different mechanisms including the convergence of residual flow in estuarine bottom-waters [Postma, 1967], lateral variations in longitudinal density currents [Nichols and Poor, 1967], the reduction in fluvial energy [Nichols et al., 1991], and salinity-induced sediment flocculation [Postma, 1967, Gibbs et al., 1989, Lick and Huang, 1993]. Within stratified environments the convergence of flow, the reduction in bottom shear stress and the suppression of turbulence, all at the edge of a salinity front, has also been observed as mechanisms for trapping and rapid deposition of suspended sediment [Geyer, 1993, Jaeger and Nittrouer, 1995, Huan-ting et al., 1982].

Water column measurements obtained by Geyer [1995] have identified the existence of a salinity front which forms during ebb tide in the Hudson River estuary whose location is consistent with the estuarine turbidity maximum(ETM). The formation of this front was also predicted by a three-dimensional numerical model applied to the Lower Hudson River Estuary by Geyer et al. [1997]. For specific river and tidal conditions the formation of this front resulted in a convergence in bottom water flow, and the focusing of sediment at a location consistent with the position of the ETM for the Hudson. In addition to an along channel convergence of flow during ebb tide,

the model also produced a lateral convergence of flow during flood tide. This lateral convergence was mainly due to asymmetry in the cross-section of the channel which promoted the formation of a transverse, westward dipping, baroclinic pressure gradient. This second trapping mechanism resulted in sediment deposition on the west side of the channel primarily to the north of the ebb deposit, between km 18 and km 25. While previous studies on the Hudson have identified high sediment accumulation rates within the ETM deposit of the Hudson [e.g. Olsen et al., 1978, Olsen, 1979, Hirschberg et al., 1996], too few samples were taken to determine how sedimentation varies both spatially and temporally within it. This knowledge is necessary in order to assess the trapping mechanisms identified by Geyer [1995] and Geyer et al. [1997].

Chemical and grain size analyses performed by Panuzio [1965], sediment facies mapping conducted by Coch [1986] and radionuclide measurements obtained by Olsen [1979] show that sediment within the ETM deposit of the Lower Hudson is composed primarily of fine, river-borne material. This type of sediment has a low sonar reflectivity and can be identified through the use of side-scan sonar [Ryan and Flood, 1996]. Side-scan sonar maps a sediment surface by sending out a fan-shaped sound beam and measuring the strength of the sound beam return. The grain size of surficial sediment as well as the topographic relief of the bottom affect the strength of this return. Coarse grained sediment produces a stronger sonar return than fine grained sediment [Ryan and Flood, 1996]. Likewise, a bottom slope facing the sonar beam produces a stronger return than a slope facing away from the sonar beam [Wright

et al., 1987, Knebel et al., 1991]. As a result side-scan sonar produces an image similar to an aerial photograph which, with some care, can be used to determine variations in sediment type as well as bottom morphology. Flood and Bokuniewicz [1986] used a side-scan sonar to investigate sediment facies and bed forms in the Lower Hudson River estuary. The location of fine-grained deposits identified by Flood and Bokuniewicz [1986] were consistent with the location of the ETM for the Hudson. Flood's study was hampered, though, due to limited coverage and the lack of supporting data concerning the local sediment types. Surficial sediment sampling used in conjunction with a more detailed side-scan survey was required to correlate side-scan patterns with the sediment facies in Lower Hudson River estuary, and to identify the spatial distribution of fine-grained deposits.

In addition to a complex spatial structure, deposition in the Lower Hudson River estuary has been observed to have a high degree of temporal variability [Hirschberg et al., 1996, Feng et al., 1998]. Panuzio [1965] estimated that 750,000 metric tons of sediment was supplied to the Hudson River estuary from upstream sources during the 1959-1960 water year. In a later study, Olsen [1979] estimated a yearly sediment load of 1.1 million metric tons to the Hudson River estuary for the 1969-1970 water year. These two studies illustrate the temporal variability in the annual load to the estuary, with the yearly sediment supply increasing by 46 percent between the two studies. Both Panuzio [1965] and Olsen [1979] observed that a majority of the river-borne sediment entering the estuary occurred over the winter and spring months

during high river discharge events. Radionuclide data collected by both Hirschberg et al. [1996] and Feng et al. [1998] suggest that sedimentation below the ETM of the Hudson varies seasonally in response to these high freshwater flows, however this response has never been quantified.

Sediment collected from below the ETM of the Hudson has been observed to contain thin laminations of clayey-silt and sandy-silt strata [Olsen et al., 1978, Olsen, 1979, Coch, 1986, Hirschberg et al., 1996, Feng et al., 1998, 1999]. Fine-scale stratigraphy within estuarine sediments is a common phenomenon whose formation has been linked to a number of river and tidal forcing processes including, variations in river discharge [Nichols et al., 1991], changes in the fortnightly tidal amplitude [Allen et al., 1980, Allen and Postmentier, 1993, Jaeger and Nittrouer, 1995] and fluctuations in current associated with the semidiurnal tidal cycle [Huang and Wang, 1987, Nio and Yang, 1991]. In the James River estuary, Nichols et al. [1991] observed layers of muddy, sand laminated beds followed by layers of thick, bioturbated mud beds. Laminated beds in the estuary resulted from the rapid accumulation of sediment during river floods while the thick, muddy, bioturbated beds were the result of slower, long-term accumulation during low river flow. At the mouth of the Amazon River, Jaeger and Nittrouer [1995] observed a thick mud layer developing as a result of strong stratification during neap tides. High flows, and the destratification of the water column during the following spring tide resulted in the partial erosion of this mud layer, as well as the formation of sandy laminations. In the Changjiang

Estuary in East China, vertical sequences of sand-mud couplets coincide with peak flow and slack water periods during the semidiurnal tidal cycle [Nio and Yang, 1991]. Nio and Yang [1991] hypothesized that muddy laminae resulted from the raining out of suspended sediment during slack water, whereas sandy laminae were produced by the transport of coarser material during peak ebb and flood flows. Sediment structure studies such as these show that fine-scale stratigraphy observed within Hudson River estuarine sediment has the potential to identify the environmental conditions conducive to deposition within the estuary.

In this study we use a high resolution side-scan survey, in conjunction with surficial sediment sampling and bottom penetrating sonar to correlate side-scan sonar patterns, and to identify the spatial distribution of sediment deposits underneath the ETM of the Hudson River estuary. Sediment cores collected from depositional environments shortly after the spring river freshet are used to identify the depositional response in the estuary to high river discharge events, and to assess the sediment trapping mechanisms identified by Geyer [1995] and Geyer et al. [1997]. An analysis of historic stream flow and sediment load data are used to develop a relationship between Hudson River discharge and fluvial sediment influx, as well as to obtain estimates for the yearly sediment loads to the estuary. Fine-scale sediment stratigraphy are used to gain insight into the depositional response underneath the turbidity maximum of the Hudson to fluvial and tidal forcing processes.

2 Methods

2.1 Study Area

The Lower Hudson River estuary and the study area are shown in Figure 1. Positions along the estuary are measured in kilometers northward along the river channel beginning at the Battery on the southern tip of Manhattan. The 1998 study area stretches from km 8 to km 25, encompassing the areas of high sediment deposition identified by Olsen [1979], as well as the position for the turbidity maximum of the estuary [Hirschberg and Bokuniewicz, 1991, Geyer, 1995, Geyer et al., 1997]. The Weehawken-Edgewater Channel runs along the west side of the Lower Hudson River estuary between km 10 and km 15. Approximately 330,000 metric tons (dry weight) of sediment are dredged annually from the Weehawken-Edgewater Channel to maintain a depth of 9 meters [Gross, 1974]. The last dredging project for the channel was conducted 4 years prior to the study during the summers of 1994 (ACOE personal communication).

2.2 Environmental Conditions

Figure 2 displays the hydrograph for the Hudson River measured at Green Island, New York (km 240) over the 1997-1998 water year. The field study took place between the 23rd and 25th of June, at the end of a 10 day, high river discharge event, and approximately three months after the 1998 spring freshet. River discharge over the

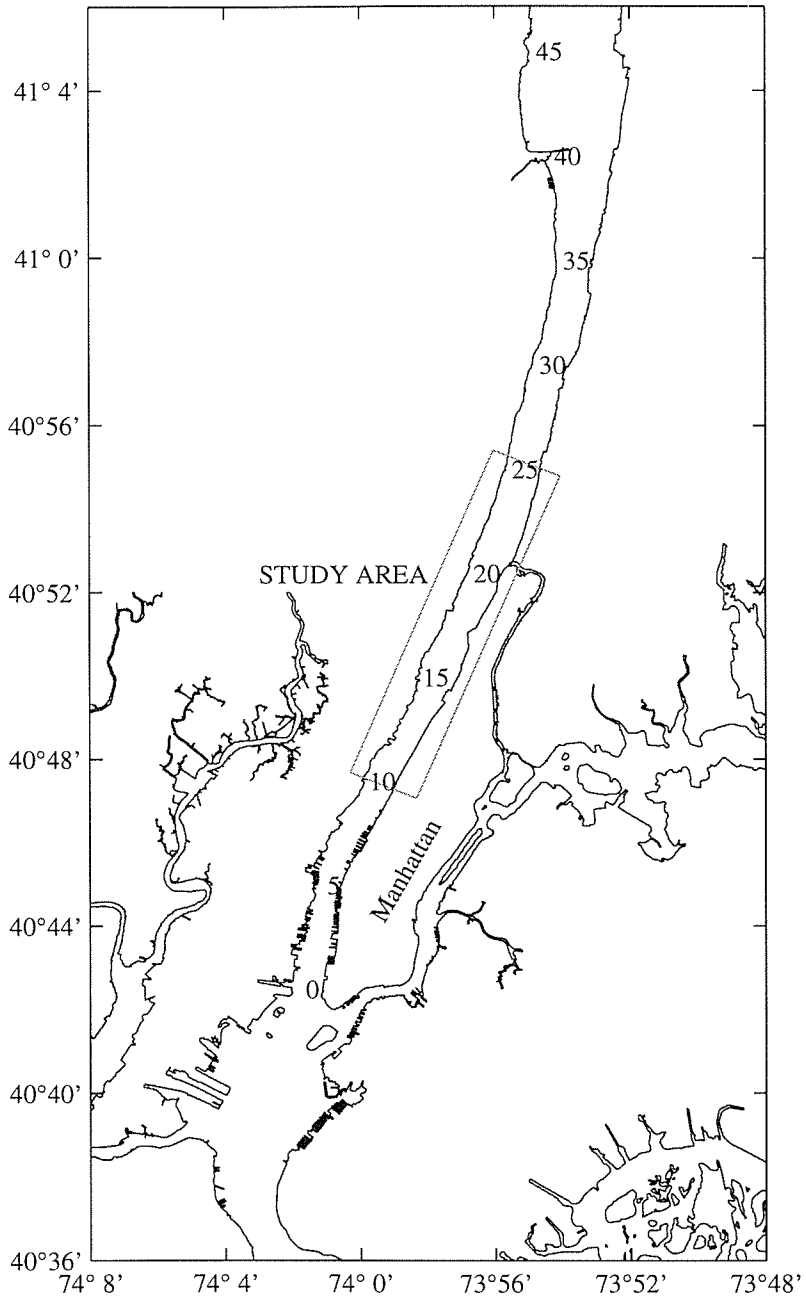

Figure 1: Map of Lower Hudson River estuary and upper New York Harbor. The gray box identifies the 1998 study area. The numbers indicate kilometers along the river, referenced to the Battery.

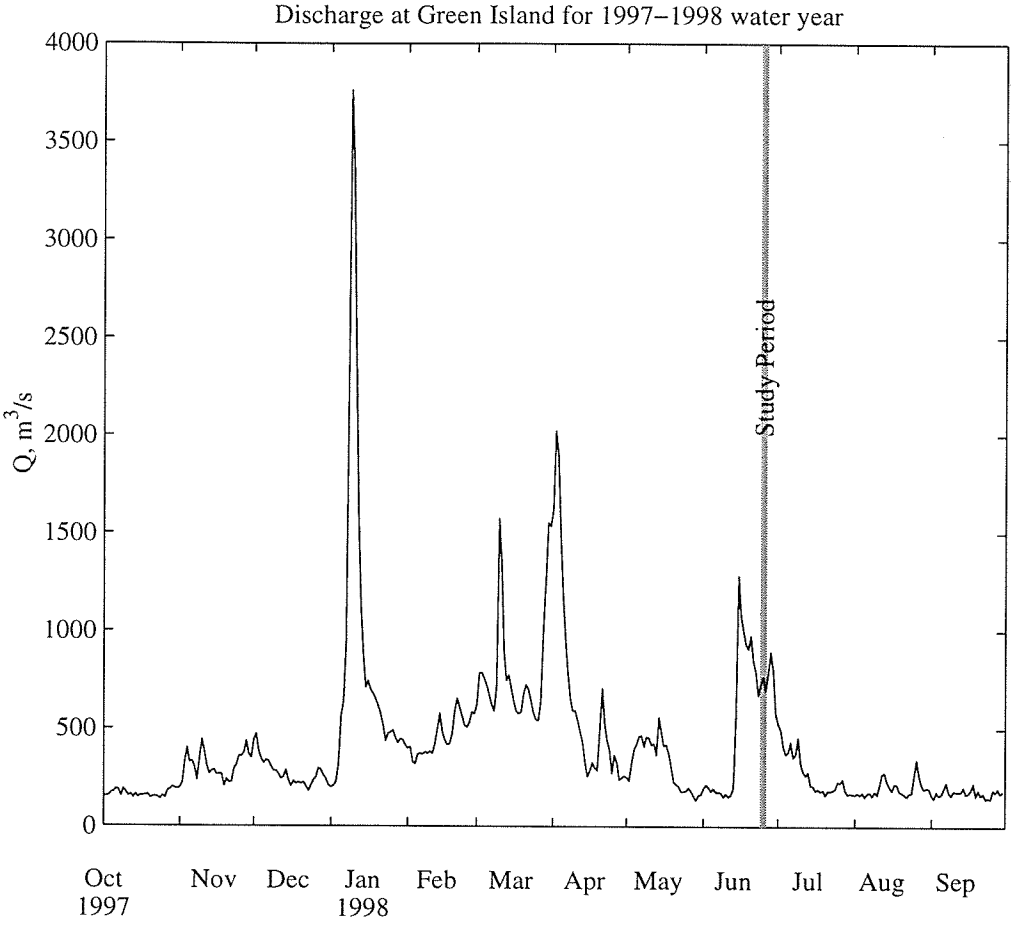

Figure 2: River discharge at Green Island, New York (240 km north of Battery), from USGS records.

spring freshet months of March and April were slightly below normal with a mean discharge of 725 m^3/s, compared to the long-term mean of 750 m^3/s [Abood, 1974]. Of particular importance in the 1997-1998 hydrograph is a high river discharge event with a 10 year return period which occurred between the 6th and 10th of January.

The estuary is strongly stratified during neap tides and well mixed during spring tides. This is true except during high river discharge events in which the estuary remains stratified for the entire spring-neap cycle [Geyer et al., In Press]. The tidal range during the study period varied between 1.6 and 2 m, reflecting spring conditions (Figure 3). Due to high freshwater flow the estuary was strongly stratified, with a maximum surface to bottom salinity difference exceeding 9 psu.

Flows are tidally dominated in the Lower Hudson River estuary with peak tidal transport during the spring-neap cycle ranging from 8,000 m^3s^{-1} to 11,000 m^3s^{-1}, compared to the the annual fresh water flow in the lower estuary of 550 m^3s^{-1} [Abood, 1974]. At normal levels of river discharge the tidally averaged flow in the Lower Hudson River estuary exhibits a characteristic two layered, two-way, counter-flowing pattern [Geyer et al., In Press, Chatwin, 1976]. This residual flow is seaward in the fresher surface water and landward in the saltier bottom water. The estuarine circulation in the estuary occurs throughout the entire spring-neap cycle, although it is strongest during neap conditions when the estuary is stratified [Geyer et al., In Press]. This residual current is maintained throughout the year within the turbidity maximum except during high river discharge events when net flow is reversed to

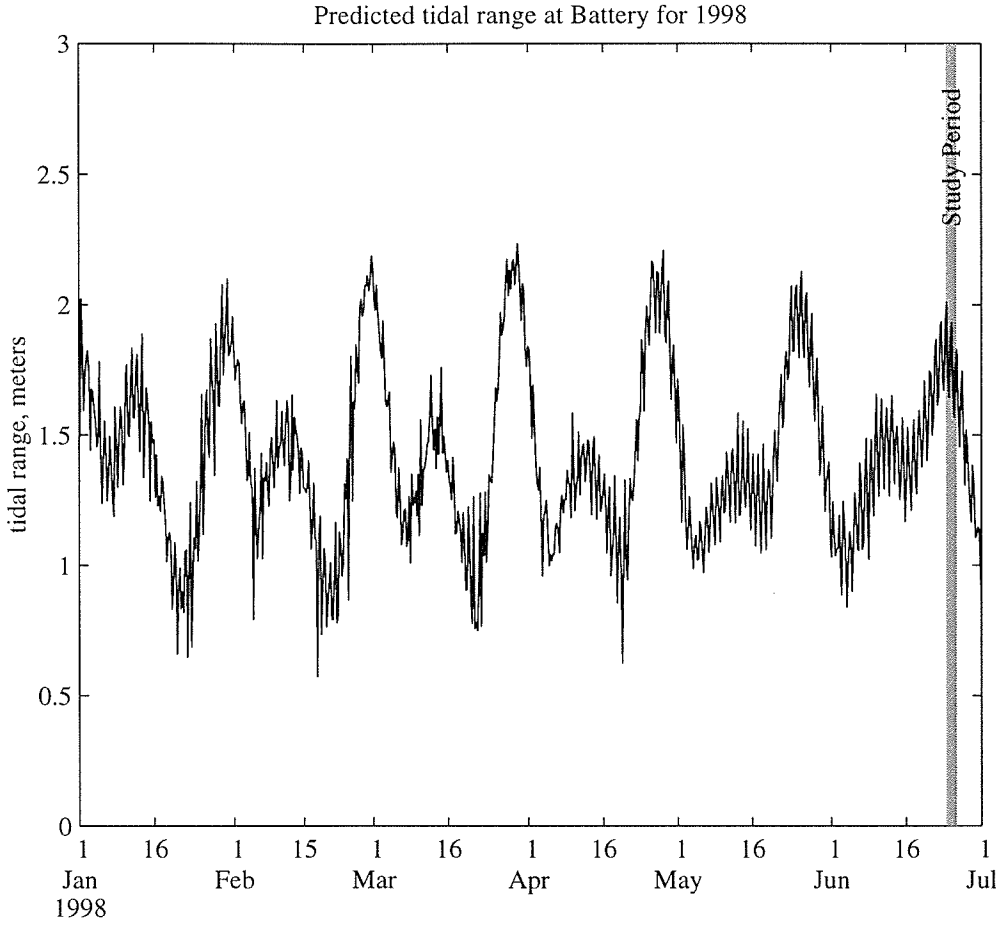

Figure 3: Tidal range at the Battery for 1998, based on NOAA predictions.

seaward at all depths.

2.3 Sampling and Analytical Procedures

Side-scan sonar and sub-bottom data were collected on the 23rd and 24th of June. The 1998 study area was divided into two sections for the side-scan survey, one south of the George Washington Bridge between km 10 and km 17 and one north of the bridge between km 18 and km 25. Each section was covered by traveling on multiple, along channel lines spaced laterally 100 meters apart. The side-scan survey was performed with a dual frequency, Edge Tech model DF 1000, side-scan sonar operating at 100 and 500 kHz. The side-scan sonar was towed at a depth of 3 meters along the port side of the vessel, with a swath width of approximately 200 meters. Simultaneously, an Edge Tech X-Star, sub-bottom profiler operating at 5 kHz was towed on the starboard side at a depth of approximately 1.5 meter. Signals for both the side-scan and sub-bottom sonar were recorded digitally along with navigation data obtained from a differential global positioning system. Paper records for both the side-scan and sub-bottom data were also printed in real time in order to determine sediment sampling locations. Boat speed ranged between 4 and 6 knots during the side-scan and sub-bottom survey.

Side-scan sonar data was processed using USGS, Xsonar and Showimage software as described by Danforth [1997]. A four pixel, across track by three pixel, along track (approximately 0.5 meter by 0.5 meter), boxcar filter was used to reduce noise in data.

Navigation data was merged with side-scan data at two minute intervals. Altitude was corrected for by visually identifying the first bottom return for each sonar scan. Slant range distortion was corrected for by assuming a flat bottom and applying a geometric correction. Beam angle effects were corrected for by balancing the mean tones of 350 along track lines evenly spaced across the entire width of the side-scan swath.

Sediment cores were collected on June 24th and 25th of 1998. The location and site identification numbers for sediment cores taken during the field study are displayed in Figure 4. Sediment samples were collected with a hydraulically dampened, gravity corer [Bothner et al., 1997]. The coring device pushed one-meter-long core barrels into bottom sediment at approximately 20 cm/s in order to reduce disruption at the sediment-water interface. Core barrels were composed of transparent polycarbonate, which allowed the viewing of sediment cores on site without extrusion. Each core was described and photographed immediately after retrieval. Cores were then capped and shipped upright to Woods Hole Oceanographic Institution where they were stored at 6 $^{\circ}C$ in order to reduce biological activity.

Once shipped to Woods Hole, x-radiographs were taken of each sediment core. After these x-radiographs were taken, selected cores were extruded and sampled for grain size and bulk density analyses. Grain size was determined by wet sieve and pipette analyses as described by Folk [1980]. Porosity measurements were obtained by comparing the sample weight before and after oven drying at 80 $^{\circ}C$. Sediment samples

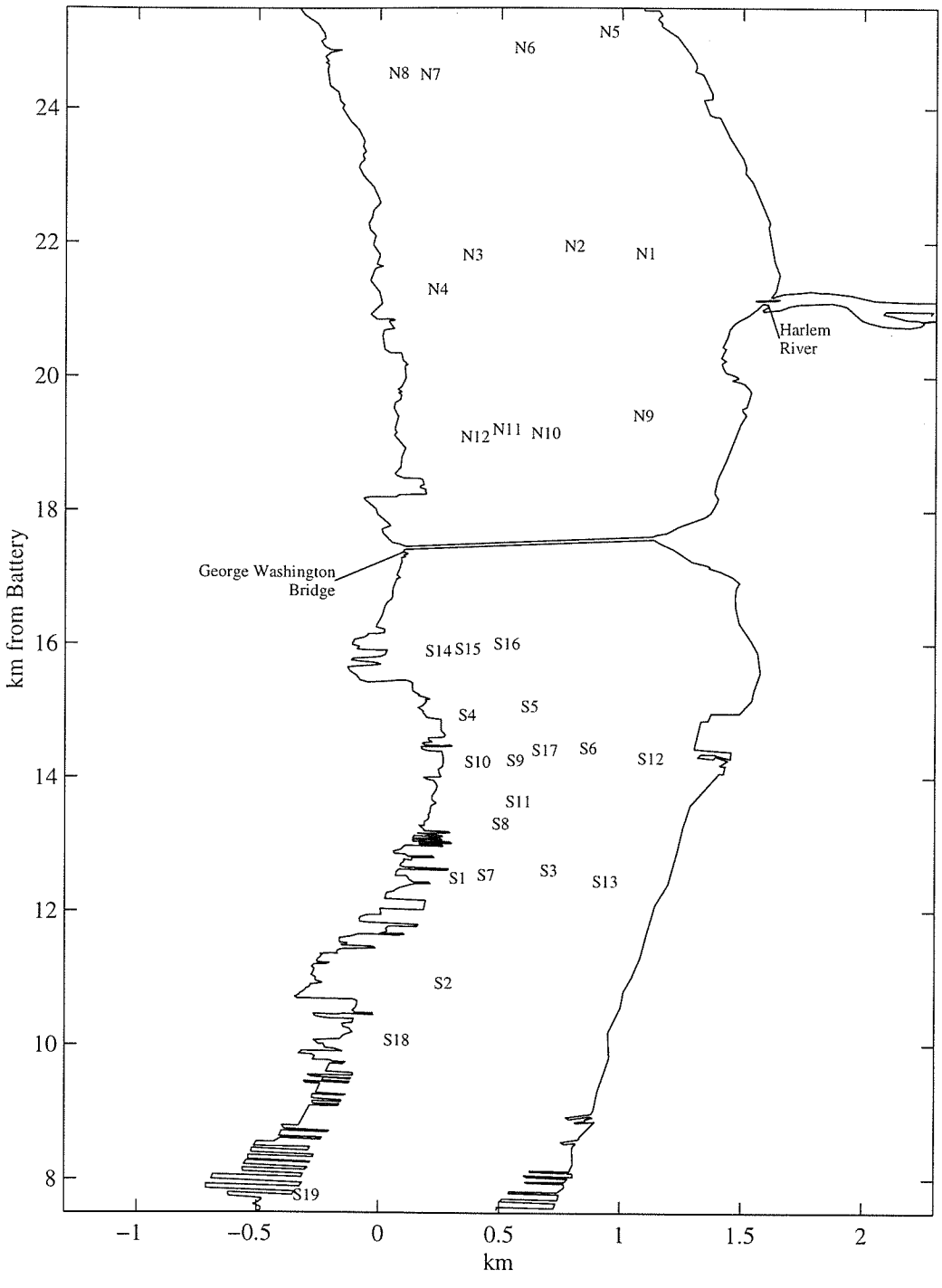

Figure 4: Location and site identification numbers for sediment cores taken during 1998 field study. The transverse scale has been exaggerated by a factor of 4.

from core S-11 were homogenized, dried and ground to a powder for radionuclide analyses. Beryllium-7 activities were determined by measuring gamma emissions of a 30 g sample at 477.6 keV by a germanium well detector.

3 Results

3.1 Side-scan Sonar

The side-scan mosaics created for the northern and southern section of the 1998 study area are shown in Figure 5 and Figure 6. Strong side-scan sonar reflections appear white on the mosaics while weak reflections and shadows appear dark. Core locations are labeled on the figures by number with the "N" or "S" omitted. A thin white line on the figures indicate the visually delineation between low and high side-scan backscatter response. Table 1 displays the grain size measurements obtained for surficial sediments collected from the northern section of the side-scan survey. The table illustrates the response of the side-scan sonar to variations in grain size and supports the visual method used to identify high and low backscatter environments. Surficial sediment collected from environments with a weak side-scan sonar return (dark areas in Figure 5) were primarily composed of fine grained material (less than 10 percent >63 μm) while surficial sediments with a strong side-scan sonar return (white areas in Figure 5) were primarily composed of coarse grained material (greater than 64 percent >63 μm).

The southern and northern side-scan mosaics identified two large, fine grained deposits within the 1998 study area. The extent of these two deposits are plotted in Figure 7 along with the bathymetry and the location of the Weehawken-Edgewater channel. The figure shows that the two deposits were located primarily on the shal-

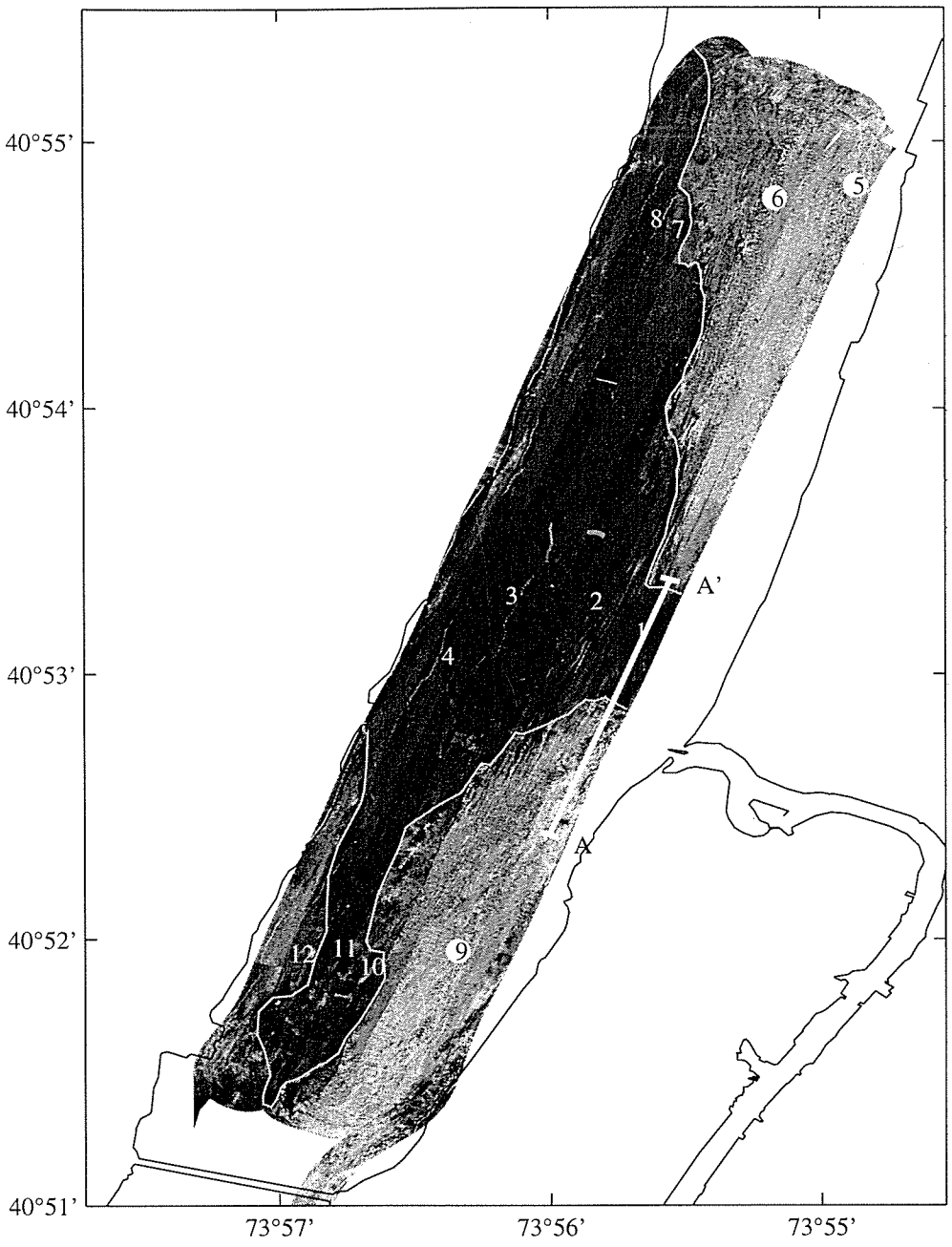

Figure 5: Side-scan mosaic for northern section. Areas of low side-scan backscatter appear dark in the figure while high side-scan backscatter areas appear white. The locations for coring sites are shown by number with the "N" omitted. The thin white line identifies the visual delineation between low and high side-scan backscatter environments. Line A-A' indicates the location of sub-bottom profile presented subsequently in Figure 8.

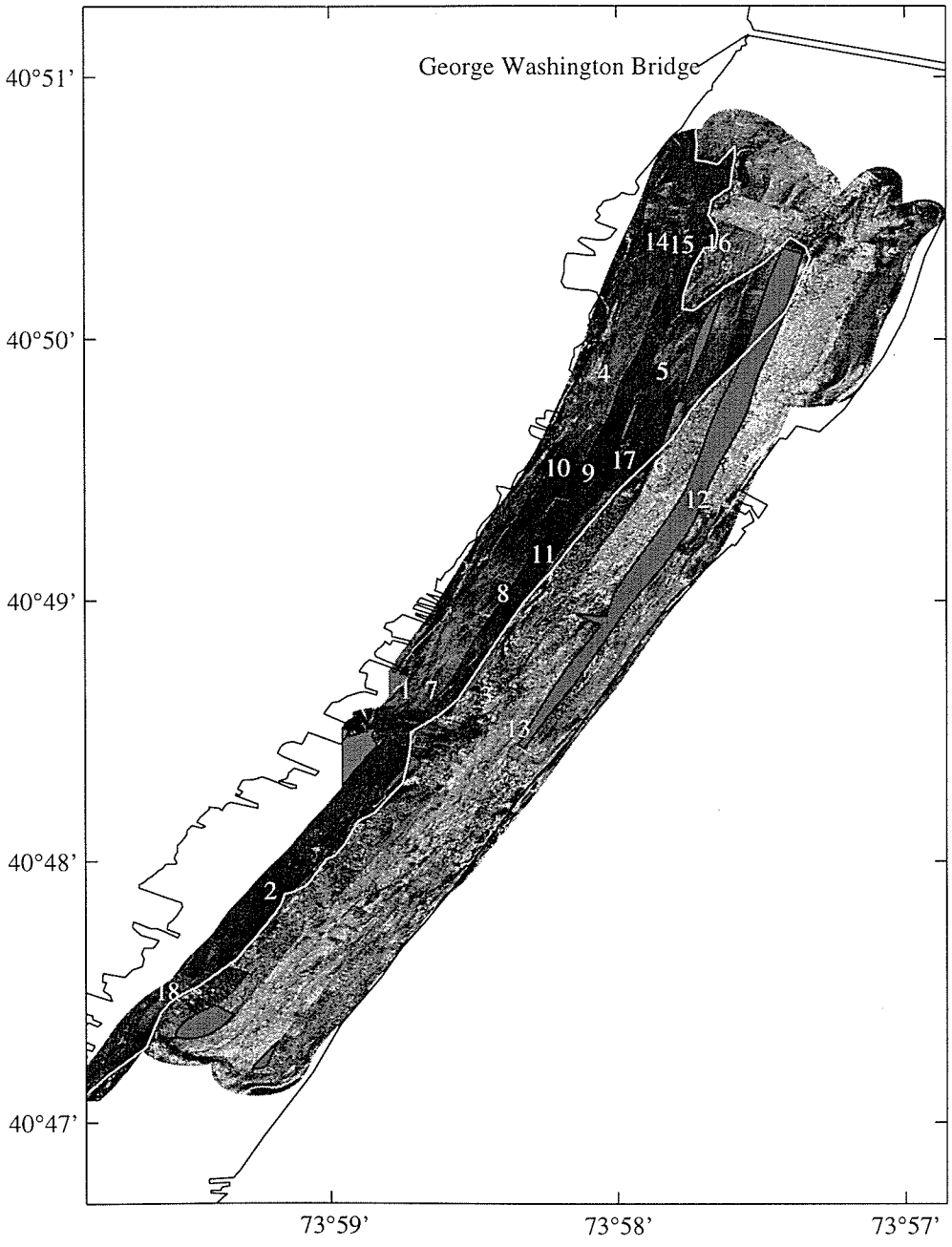

Figure 6: Side-scan mosaic for southern section. Problems in data recording resulted in small areas with no side-scan sonar coverage. These areas are shown as uniform gray patches with black borders in the figure. The thin white line identifies the visual delineation between low and high side-scan backscatter environments. The locations for coring sites are shown by number with the "S" omitted.

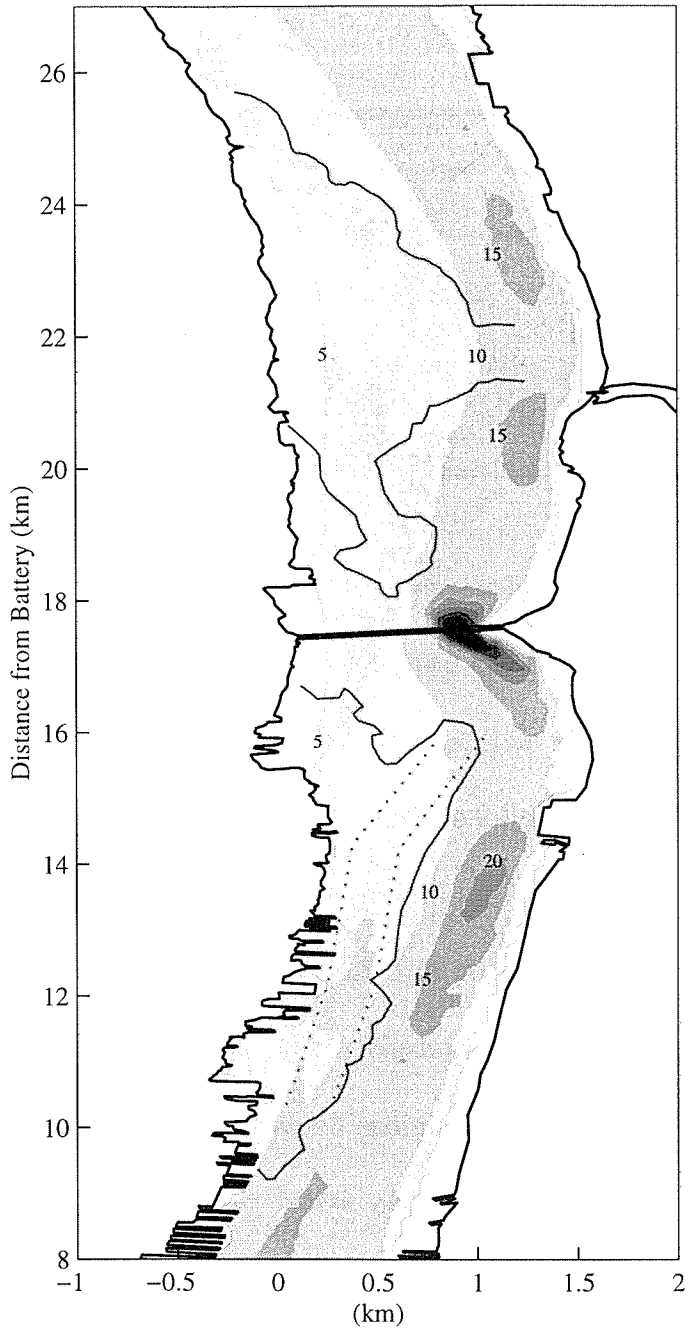

Figure 7: Channel bathymetry (in meters) for the 1998 study area based on USGS-NOS bathymetry records. The extent of the two fine grained deposits identified by the side-scan survey are displayed as black lines in the figure. The dotted line plots the location of the Weehawken-Edgewater channel. The transverse scale in the figure is exaggerated by a factor of 3.

Table 1: Grain size measurements for top 2 cm of sediment from northern section cores.

Core Number	Backscatter Response	Percent Coarse (>63 μm)	Core Number	Backscatter Response	Percent Coarse (>63 μm)
N-1	Low	9.2	N-7	Low	4.1
N-2	Low	3.2	N-8	Low	1.2
N-3	Low	1.4	N-9	High	87.9
N-4	Low	2.4	N-10	Low	3.1
N-5	High	84.3	N-11	Low	2.1
N-6	High	89.3	N-12	High	64.2

lower, west side of the channel. The southern deposit began at km 9, and was coincident with the Weehawken-Edgewater channel until km 15. North of km 15 the southern deposit widened and divided into two branches. The western branch followed the western shore while the eastern branch continued to follow the Weehawken-Edgewater channel. Both of these branches ended at around km 16.

The second fine grained deposit identified in the study area was located in the northern section, just north of the George Washington Bridge. The southern end of this deposit was a tongue of fine grained sediment approximately 200 meters wide extending from km 18 to km 20. North of km 20 the deposit widened, until it stretched almost the entire width of the channel at km 22, just upstream from the Harlem River. North of km 22, the deposit began to retreat back towards the west side of the channel, thinning until it terminated at km 25.

3.2 Sub-bottom Sonar

The sub-bottom sonar data displayed very different patterns for areas with high and low side-scan sonar backscatter. Figure 8 shows the sub-bottom sonar data collected along the line A-A' displayed on the mosaic of the northern section in Figure 5. The sonar data in Figure 8 illustrates the differences in bottom topography and sub-bottom stratigraphy observed in and out of the fine grained deposits. Bottom topography within fine grained environments was flat with relatively little relief. Sub-bottom data collected from these regions revealed horizontal stratigraphy parallel to the bathymetry, suggesting a modern depositional environment. Sub-bottom sonar often only penetrated a few centimeters within these fine grained deposits. Methane gas found in sediments taken from these areas (see Section 3.3) has been observed to have a high acoustical impedance [LeBlanc et al., 1992] and most likely explains the low sub-bottom sonar penetration in these areas.

Bottom topography outside of the two fine grained deposits was observed to have much more relief. Sub-bottom sonar images collected from these regions often contained transverse bed forms between 0.5 and 1.5 meters in height and between 9 and 16 meters in length. The sub-bottom sonar data in Figure 8 show that these bed forms often cut through the underlying stratigraphy, suggesting that these features were the result of erosion.

Patterns in the sub-bottom data suggest that areas of low side-scan backscatter (containing fine grained surficial sediment) indicate depositional conditions whereas

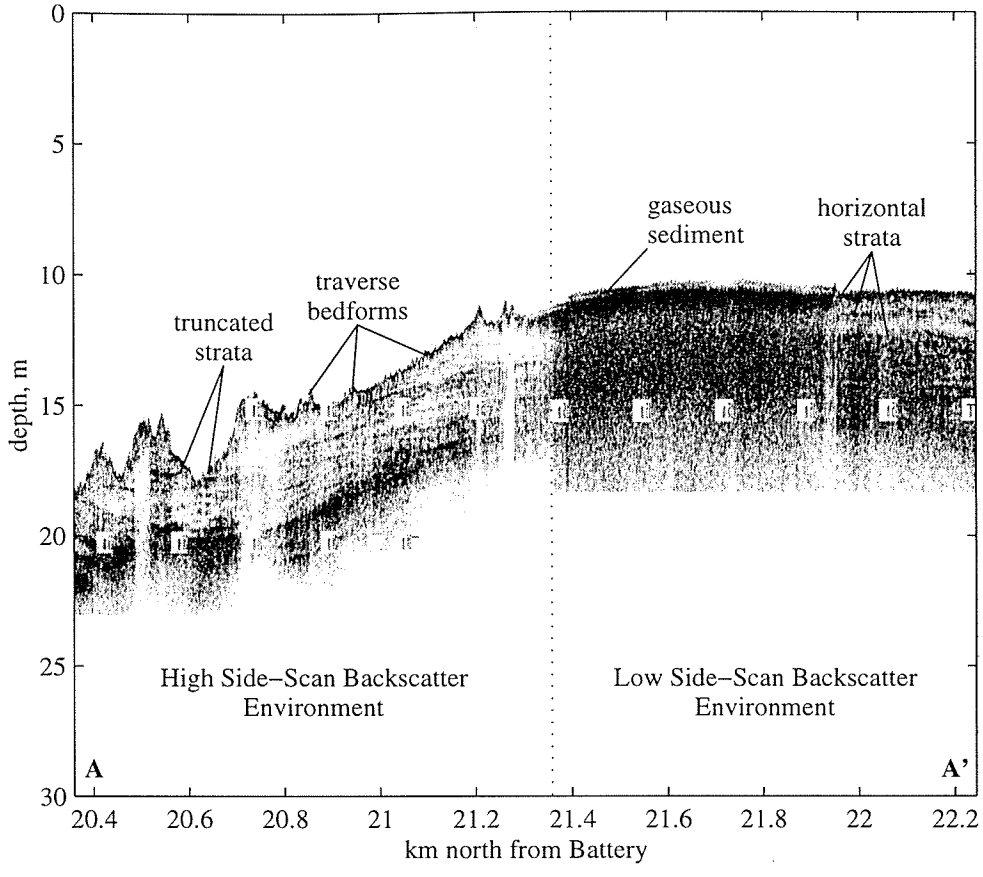

Figure 8: Typical sub-bottom profile for low and high side-scan backscatter environments. Sonar data was collected along the A-A' line displayed on the mosaic of the northern section in Figure 5.

areas of high side-scan backscatter (containing coarser grained surficial sediment) indicate areas presently undergoing erosion.

3.3 Sediment Characteristics

Patterns in sub-bottom sonar data from high and low side-scan backscatter environments revealed two different sedimentary regimes. Sediment cores collected from

these two environments contained distinctly different colors of surficial sediment, as well as different sedimentary structures.

Figure 9 displays the photographs taken of two cores (N-3 and S-11), collected from within the two fine-grained deposits identified by the side-scan survey. The cores contained a layer of fine, olive-brown sediment between 1 and 42 cm in thickness. Below this layer, the sediment abruptly changed in color to black and then gray. It has been suggested that these color changes in Hudson sediment are due to diagenic processes in which oxidized sediment containing iron hydroxides (olive-brown) has been reduced over time to iron-monosulfide (black) and then to disulfide (gray) [Olsen, 1979, Biggs, 1967, Van Straaten, 1954].

The x-radiograph negatives for core S-11 and N-3 are displayed in Figure 10. X-radiographs taken of cores from inside the two fine-grained deposits revealed well preserved, fine-scale stratigraphy in the deposits oxidized sediment. Sediment within this oxidized layer contained alternating layers of fine and coarse material. Fine grained strata (darker x-rays) were on the order of a centimeter thick and composed primarily of clayey silts (less than 10 percent >63 μm). The coarser laminations (lighter x-rays) were much thinner, on the order of a millimeter in thickness and composed primarily of sandy silts (20 to 30 percent >63 μm). Stratigraphy below the oxidized sediment layer was much more disturbed. Numerous burrows were present in these sections of the cores as well as methane gas bubbles, shown as dark pock marks on the x-radiograph. The oxidized state of the top 1 to 42 centimeters of

Figure 9: Photographs of core S-11 and core N-3. The pattern of a surficial olive brown layer followed by layers of black and then gray sediment was typical for cores collected from the two fine-grained deposits. Resuspended sediment in the overlying water was evident in both cores, particularly core S-11. The core barells are 11 cm wide.

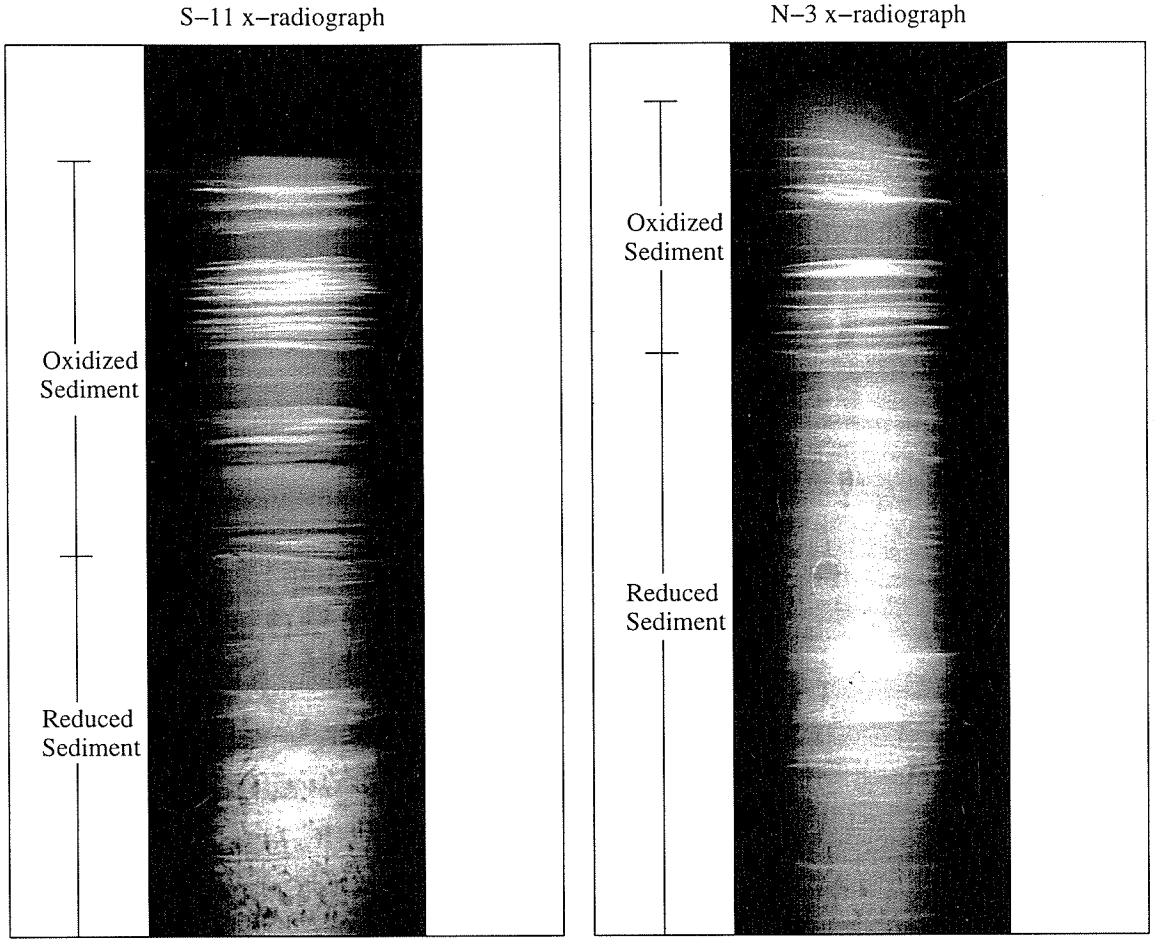

Figure 10: X-radiograph negatives of core S-11 and core N-3. Fine-grained sediment appears gray on the negative while coarser sediment appears white. The designation of oxidized and reduced sediment is based on color changes indicated in Figure 9. Stratigraphy is well preserved within the cores oxidized sediment. Sediment below this oxidized layer has been disturbed by burrows and methane gas.

sediment within the two fine grained deposits, along with the lack of bioturbation in this oxidized layer, suggests that this sediment had been recently deposited some time within the preceding year. The timescale of this deposition was confirmed by radionuclide dating (See Section 3.4).

The patterns observed in sediment structure and color in cores collected from outside of the two fine-grained deposits were much different from the cores collected from inside of these deposits. Sediment cores from high side-scan backscatter environments such as N-9 and S-3 (Figure 11) contained a coarse surficial layer ranging from 1 cm to 10 cm thick. The x-radiographs of these cores (Figure 12) showed that this coarse layer contained very little structure. The coarse texture and limited structure in this sediment suggest that this surficial layer was a lag deposit, the result of fine material winnowed over time.

Sediment below this lag layer was much finer with alternating layers of clayey silts and sandy silts. This stratigraphy was similar to that found in the oxidized sediment of the two fine grained deposits. The fine-scale structure was more disturbed though, reflecting older sediment which had been disturbed by bioturbation and gas diffusion. The similarities in stratigraphy between sediment underlying the observed lag layer and the oxidized sediment in cores such as S-11 and N-3 suggest that sediment which is presently being eroded from high backscatter environments was previously deposited under similar conditions as those now occurring in the two fine-grained deposits.

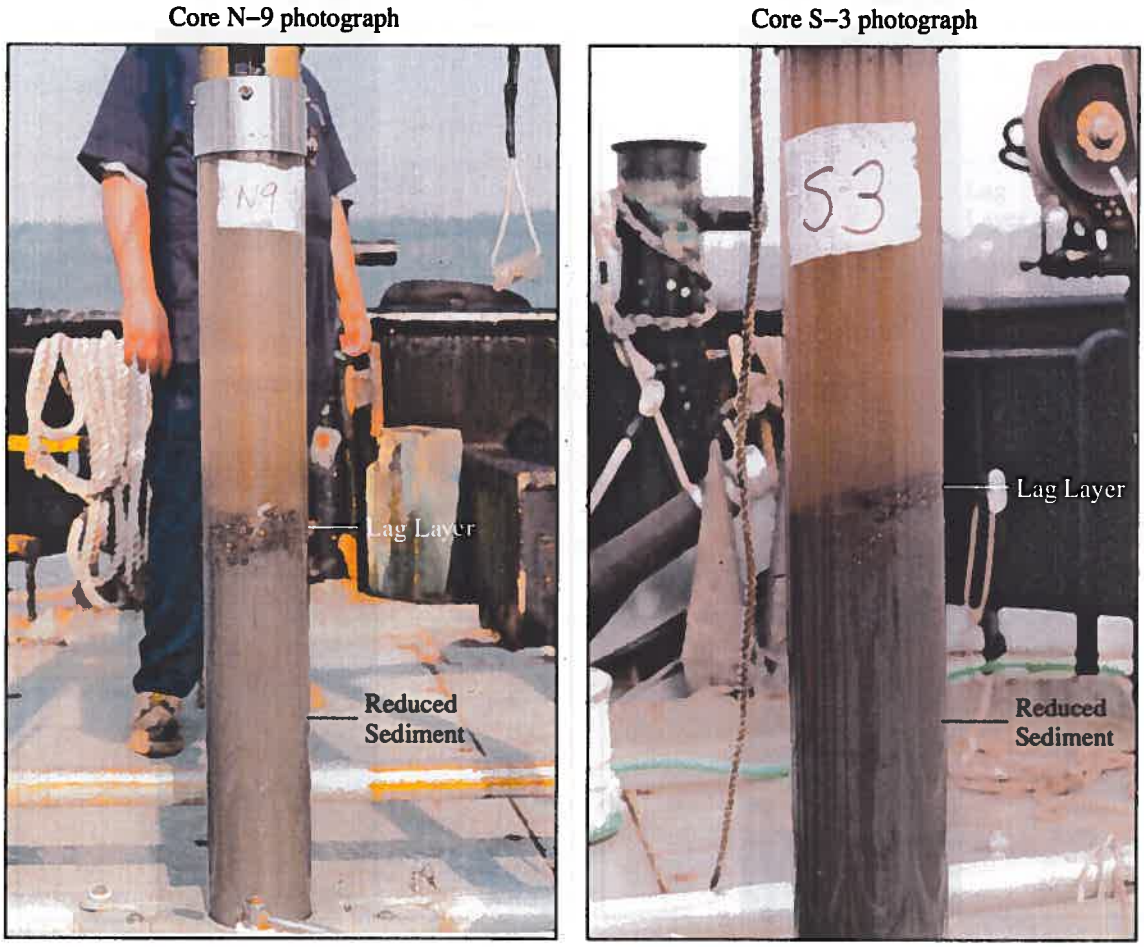

Figure 11: Photographs of core N-9 and core S-3. The surficial lag layer followed by finer, gray sediment was typical for cores collected from high side-scan backscatter environments.

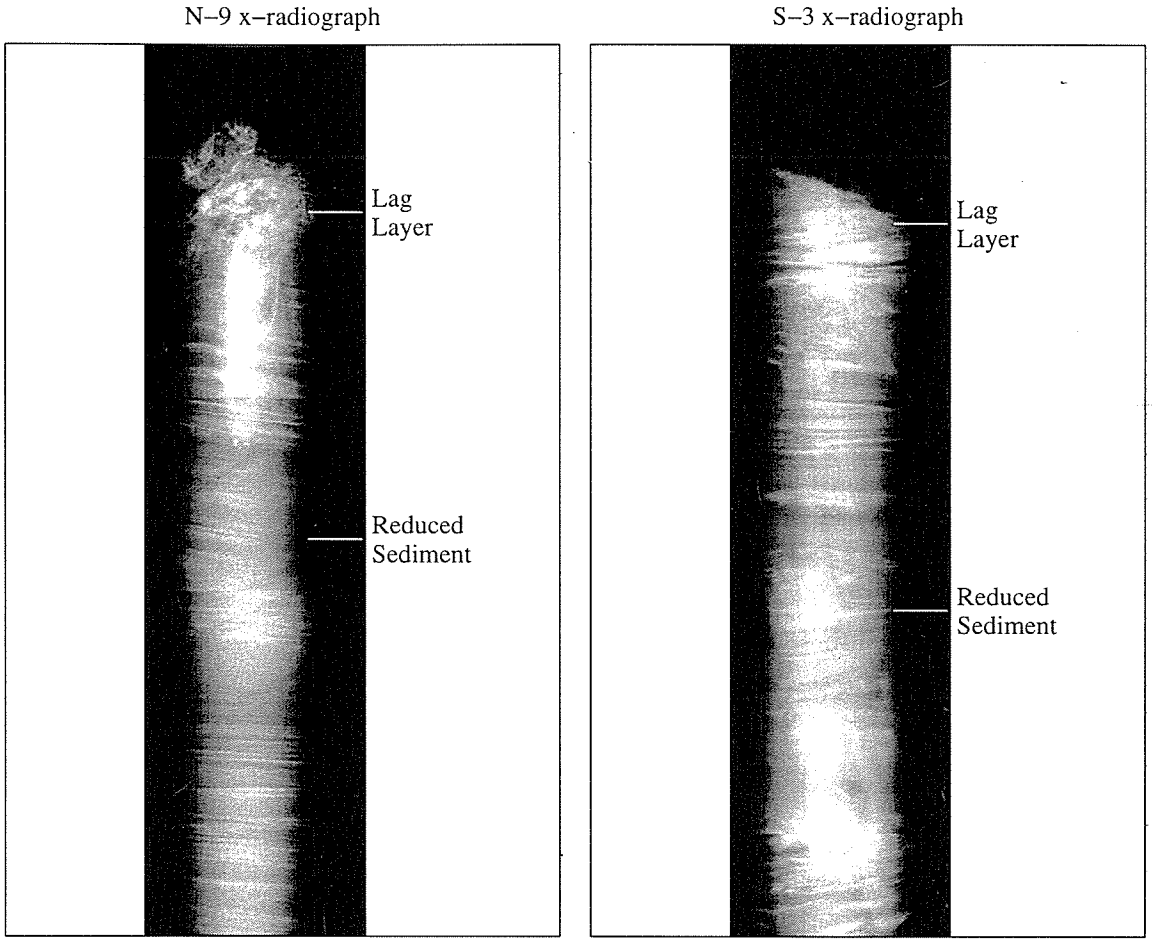

Figure 12: X-radiograph negatives of core N-9 and core S-3. Sediment within the lag layers of these cores is coarse with very little structure. Sediment below this lag layer is much finer, containing fine-scale stratigraphy which has been disturbed by burrows and gas production.

3.4 Timescale of Sediment Deposition

The oxidation and the preservation of fine-scale stratigraphy in the surficial sediments from the two fine-grained deposits suggests that this sediment may have been recently deposited. The activities of the short lived, radionuclide Be-7 (half-life of 53 days) were measured in this sediment to better quantify the time of sediment deposition.

Be-7 is a cosmogenic radionuclide supplied to the Hudson River estuary from the atmosphere. Its specific activity in the estuary is governed primarily by regional precipitation, reaching a maximum during months of high precipitation in the spring and a minimum during periods of low precipitation in the late summer and early fall [Olsen et al., 1986]. Based on Be-7 activities measured from suspended sediment collected in the Lower Hudson River estuary during July of 1981, Olsen et al. [1986] estimated an activity of 2800 pCi/kg for water column sediment. These activities are similar to the measurements presented by Feng et al. [1999] in which it was estimated that the Be-7 activity for suspended sediment in ETM of the Hudson was approximately 2000 pCi/kg during August of 1995. Once suspended sediment is deposited in the Hudson, its Be-7 activities begin to decrease rapidly due to the short half life of Be-7. The presents of measurable Be-7 in Hudson sediment indicates that the sediment has been in direct contact with the overlying water within the last six months. This makes Be-7 a useful tracer in identifying recently deposited sediment.

Results from the Be-7 analysis for core S-11 are shown in Figure 13. Be-7 activities were relatively high in the oxidized sediment of core S-11, ranging from 1700 pCi/kg

to 3100 pCi/kg. Be-7 activity below this layer was undetectable, indicating much older material. The activity of Be-7 within the oxidized sediment of core S-11 are comparable to the activities found in suspended sediment by Olsen et al. [1986] and Feng et al. [1999]. This indicates this oxidized sediment was recently deposited, probably less than the 53 day half life of Be-7 and certainly within the last six months.

3.5 Sediment Inventory

The presence of Be-7 in the surficial sediment of core S-11, which was both oxidized and contained well preserved strata, indicates that these two patterns can be used in combination to estimate the mass of sediment deposited in the study area during the spring of 1998. Figure 14 displays the depths of the spring deposit as determined by oxidized sediment thickness, and confirmed by the extent of well preserved, fine-scale stratigraphy. The dotted rectangles in the figure represent the areas used to estimate sediment inventory for the northern and southern deposits. Sediment inventory was obtained by the sum of all deposit depths times their respective rectangular areas. The deposit depth was given a value of zero for areas outside of the identified rectangles. Based on the results from Figure 14 the volume of new sediment deposited within the study area was estimated as 460,000 m^3. Using a sediment bulk density of 650 kg/m^3 [Panuzio, 1965] this is equivalent to a mass of approximately 300,000 metric tons. The distribution of this sediment inventory was relatively even between the two deposits, with 160,000 metric tons estimated for the southern deposit and 140,000

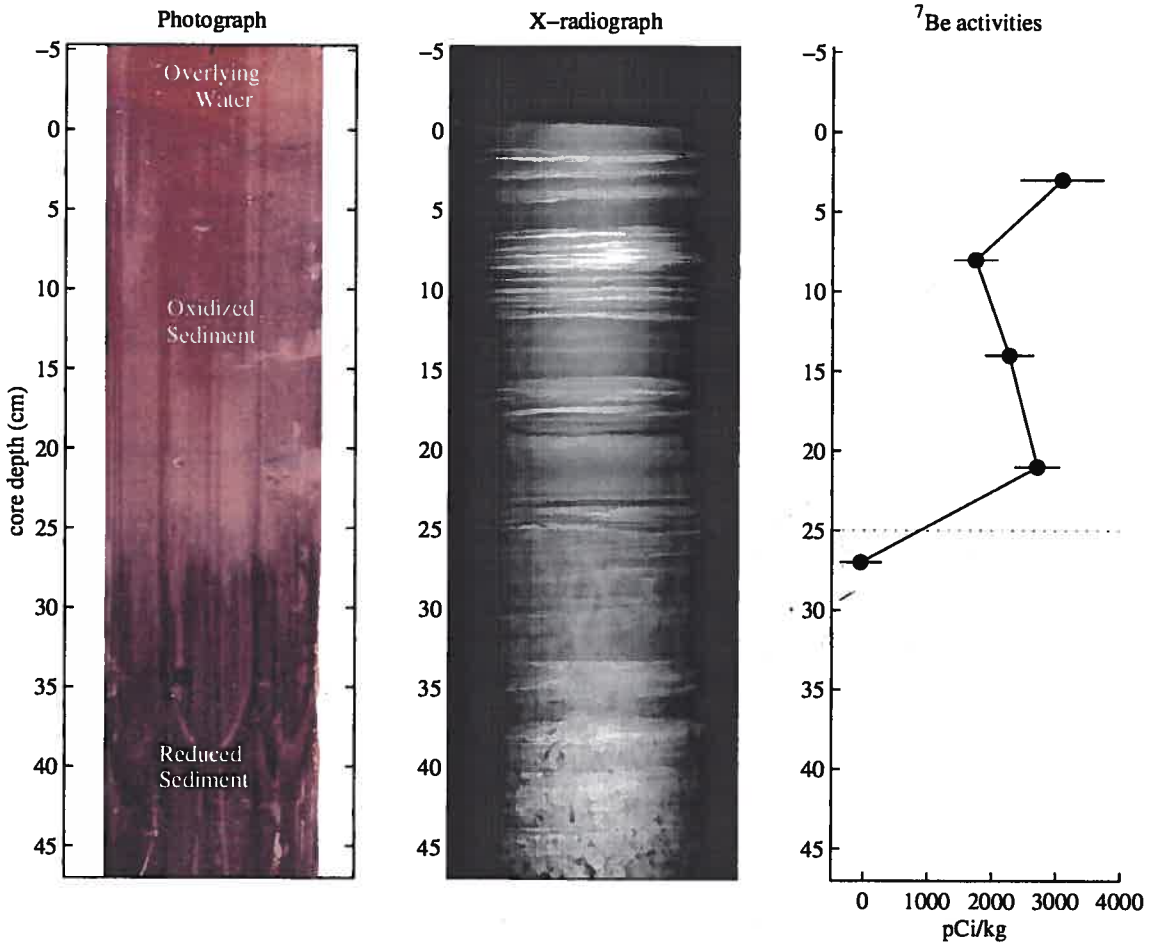

Figure 13: Photograph, x-radiograph negative and Be-7 activities for core S-11. The high Be-7 activities observed in the oxidized sediment of core S-11 indicates that this sediment had been recently deposited, most likely within the preceding two months.

metric tons estimated for the northern deposit.

3.6 River-borne Sediment Fluxes

Figure 15 and Figure 16 present historic USGS daily discharge and sediment load data collected from the Mohawk River at Cohoes and Upper Hudson River at Waterford, just upstream from the junction of the two rivers at km 250. These two rivers account for approximately 70 percent of the freshwater flow past the Battery (km 0), and are the major contributors of sediment to the estuary [Abood, 1974, Olsen, 1979]. There is a distinct increase in the slope of the log-log regression line between water discharge and sediment load for both the Mohawk and Upper Hudson rivers, occurring at 500 and 400 m^3/s respectively. This rapid increase in the rate of sediment transport at high river flows is common for rivers in the Eastern United States [Nash, 1991]. It has been suggested by Nash [1991] that this phenomenon is due to the exposure of more easily erodible material by the destruction of bank stabilizing vegetation and the erosion of river lag deposits. The exponents obtained for the Mohawk and Upper Hudson at low discharges are typical for rivers in the Mid-Atlantic [Nash, 1991], however the exponents obtained for high river discharges significantly exceeded the values of east coast rivers obtained by Nash [1991]. These higher values were comparable to the exponents obtained by Nash [1991] for semi-arid rivers of Arizona (1.82-3.02), where soil is not protected by vegetation. These high exponents cause high flow events in the Mohawk and Upper Hudson rivers to contribute disproportionately to the annual

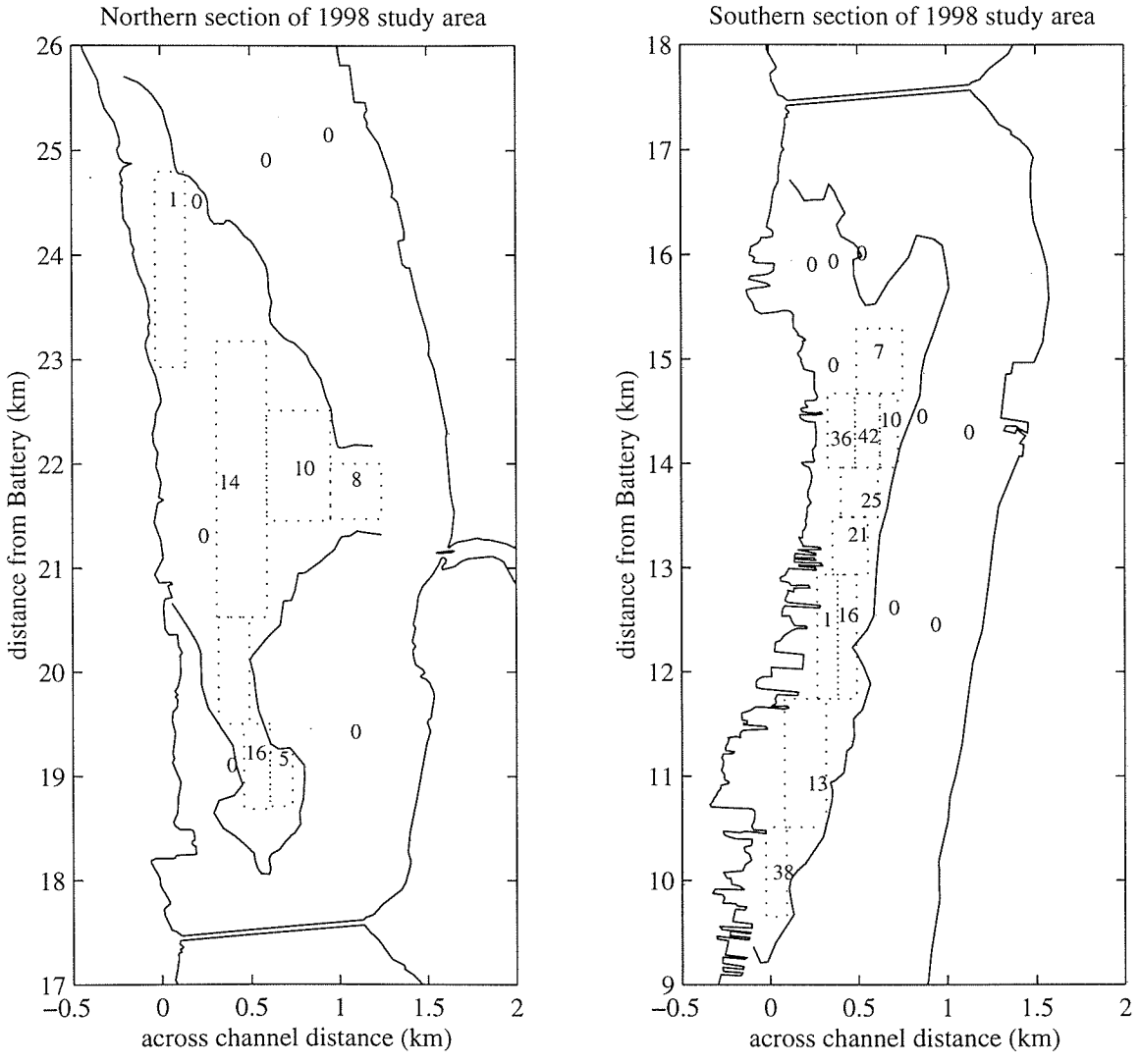

Figure 14: Depth of the 1998 spring deposit as determined by sediment thickness of oxidized layer and confirmed by extent of well preserved fine-scale stratigraphy. The numbers in the figure represent the deposit depth observed at the location. The spatial extent of the two fine-grained deposits are presented as black lines in the figure. Dotted rectangles represent areas used to estimate sediment inventory for the northern and southern deposits.

sediment load to the estuary.

The annual sediment load calculated using complete years of available, USGS daily sediment load data for the Mohawk River at Cohoes and the Upper Hudson River at Waterford are displayed in Table 2 and Table 3, along with the load predictions obtained by applying the power law relationships from this study to historic daily discharge data. The tables show that the actual and predicted annual loads compare favorably for both rivers, with the actual measured annual loads falling well within the error estimates for the predicted loads. The error bounds in Table 2 and Table 3 were obtained by taking the sum of the daily error estimates for sediment load based on 50 percent confidence for all the days within the given water year. This is a conservative estimate for the error in the predicted annual load since it assumes that the individual daily errors within a water year are correlated.

Table 2: Annual loads measured by the USGS from the Mohawk River at Cohoes compared to predicted annual sediment loads based on power-law relationship in Figure 15. The table shows that the actual sediment loads fall within the conservative error bounds for the predicted loads.

Water Year	Actual Annual Load metric tons x 10^6	Predicted Annual Load metric tons x 10^6	Error Bounds for Predicted Loads metric tons x 10^6
1954-1955	0.19	0.13	0.07 to 0.24
1955-1956	0.78	0.66	0.38 to 1.14
1956-1957	0.08	0.06	0.03 to 0.11
1957-1958	0.16	0.12	0.07 to 0.21
1958-1959	0.17	0.13	0.07 to 0.24
1976-1977	0.75	0.80	0.46 to 1.38

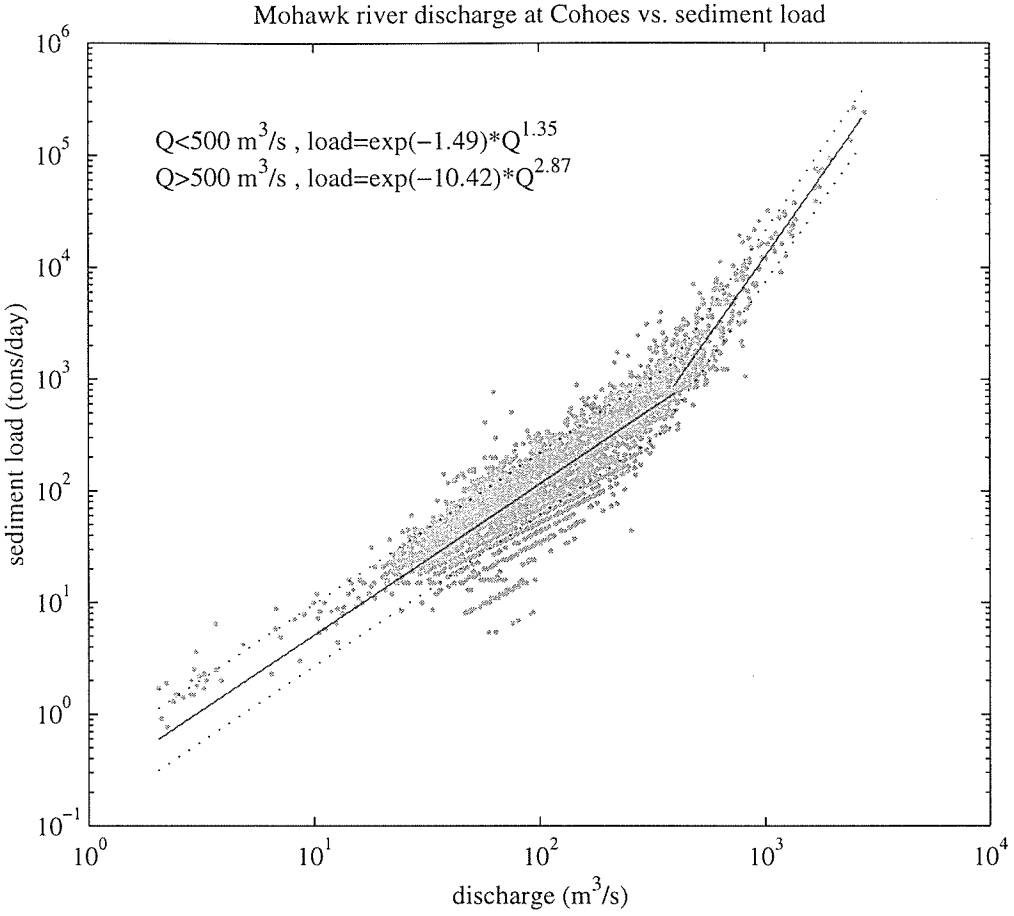

Figure 15: USGS daily river discharge and daily sediment load data collected from the Mohawk River at Cohoes, New York during 1954-1959 and 1976-1979. The solid lines in the figure represent the regressions for discharges above and below 500 m^3/s. The dotted lines represent error estimates for 50 percent confidence. The banded structure in the USGS data for low sediment loads is the result of rounding suspended sediment concentrations to whole increments of mg/l [Edwards and Glysson, 1988].

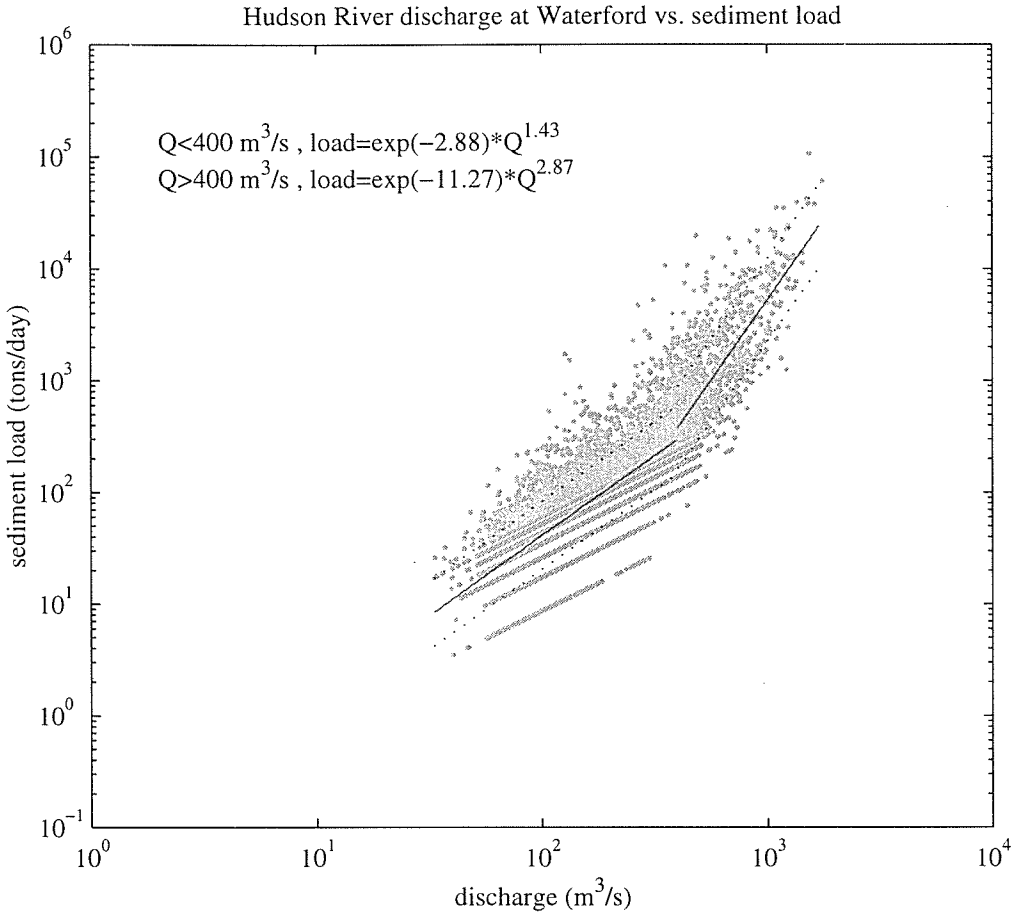

Figure 16: USGS daily river discharge vs. daily sediment load data collected from the Upper Hudson River at Waterford, New York between 1976 and 1994. The solid lines in the figure represent the regressions for discharge above and below 400 m^3/s. The dotted lines represents error estimates for 50 percent confidence. The banded structure in the USGS data for low sediment loads is the result of rounding suspended sediment concentrations to whole increments of mg/l [Edwards and Glysson, 1988].

Table 3: Annual loads measured by the USGS for the Upper Hudson River at Waterford compared to predicted annual sediment loads obtained by the power-law relationship in Figure 16. The table shows that the actual sediment loads fall within the conservative error bounds for the predicted loads.

Water Year	Actual Annual Load metric tons x 10^6	Predicted Annual Load metric tons x 10^6	Error Bounds for Predicted Loads metric tons x 10^6
1976-1977	0.35	0.19	0.08 to 0.43
1977-1978	0.19	0.13	0.06 to 0.28
1978-1979	0.31	0.19	0.08 to 0.44
1979-1980	0.09	0.07	0.03 to 0.14
1991-1992	0.09	0.06	0.03 to 0.14
1992-1993	0.21	0.18	0.08 to 0.42

Annual sediment load predictions based on the results from Figure 15 and Figure 16 also compare favorably to the annual loads measured by Panuzio [1965] and Olsen [1979]. Figure 17 displays the estimated annual sediment load to the Hudson River estuary obtained by applying the power law relationships from this study to 52 years of historic daily stream flow data from the Mohawk and Upper Hudson rivers. The annual sediment load predictions for the 1959-1960 and 1976-1977 water years were 0.83 x 10^6 and 0.99 x 10^6 metric tons, respectively. These predictions are relatively close to the annual sediment loads of 0.75 x 10^6 and 1.10 x 10^6 metric tons calculated independently by Panuzio [1965] and Olsen [1979]. It is interesting to note that the sediment flux studies performed by Olsen [1979] and Panuzio [1965] were conducted on the highest and second highest sediment load years predicted using the 52 year river discharge record. The mean yearly sediment load to the estuary based

on these two studies, therefore, is most likely a substantial overestimate of the average annual sediment load to the estuary.

Figure 18 displays the hydrograph for the 1997-1998 water year, along with the cumulative sediment load to the Hudson River estuary based on the river discharge and sediment load relationships obtained in this study. Approximately 0.57 x 10^6 metric tons of river-borne sediment was supplied to the estuary over the 1997-1998 water year. Almost all of this annual sediment load, approximately 95 percent, was supplied prior to the June of 1998 field study. Figure 18 shows that sediment load is particularly sensitivity to high river flows. Approximately 60 percent of the annual river-borne sediment load to the estuary was supplied in just four days during the high river discharge event in January.

Based on the results from Section 3.5 and the conservative error bounds in Figure 18, between 30 and 98 percent of the 1998 fluvial sediment input to the Hudson River estuary can be accounted for by the spring inventory of the northern and southern deposits. These percentages are similar to those found for the James River estuary where it has been estimated that 45 to 92 percent of the fluvial input is deposited within the estuary [Nichols et al., 1991].

3.7 Fine-Scale Sediment Structures

Figure 19 displays the x-radiographs for core S-9 and S-11. These cores were both located within the southern deposit approximately 1 km apart. The thickness of the

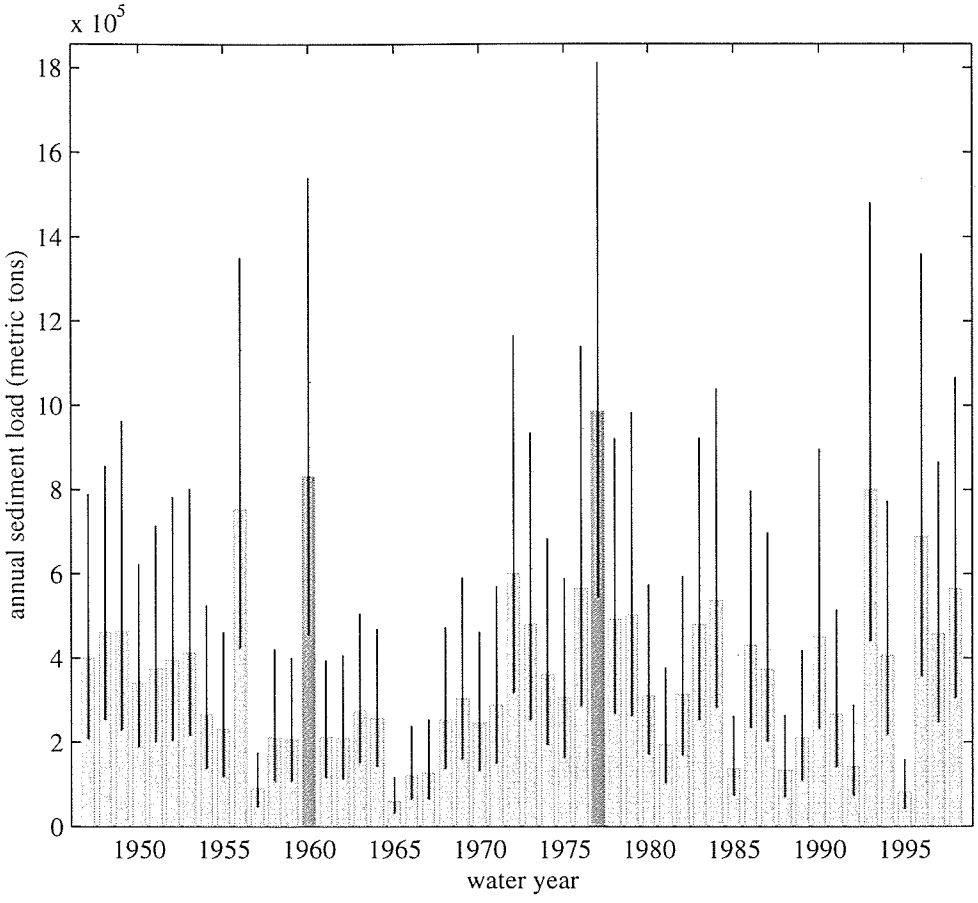

Figure 17: Annual sediment load to the Hudson River estuary obtained by applying discharge and sediment load relationships to USGS historic stream flow data. The darker bars represent years in which Panuzio [1965] and Olsen [1979] performed separate sediment flux studies on the estuary. The vertical lines represent conservative error estimates for the predicted load.

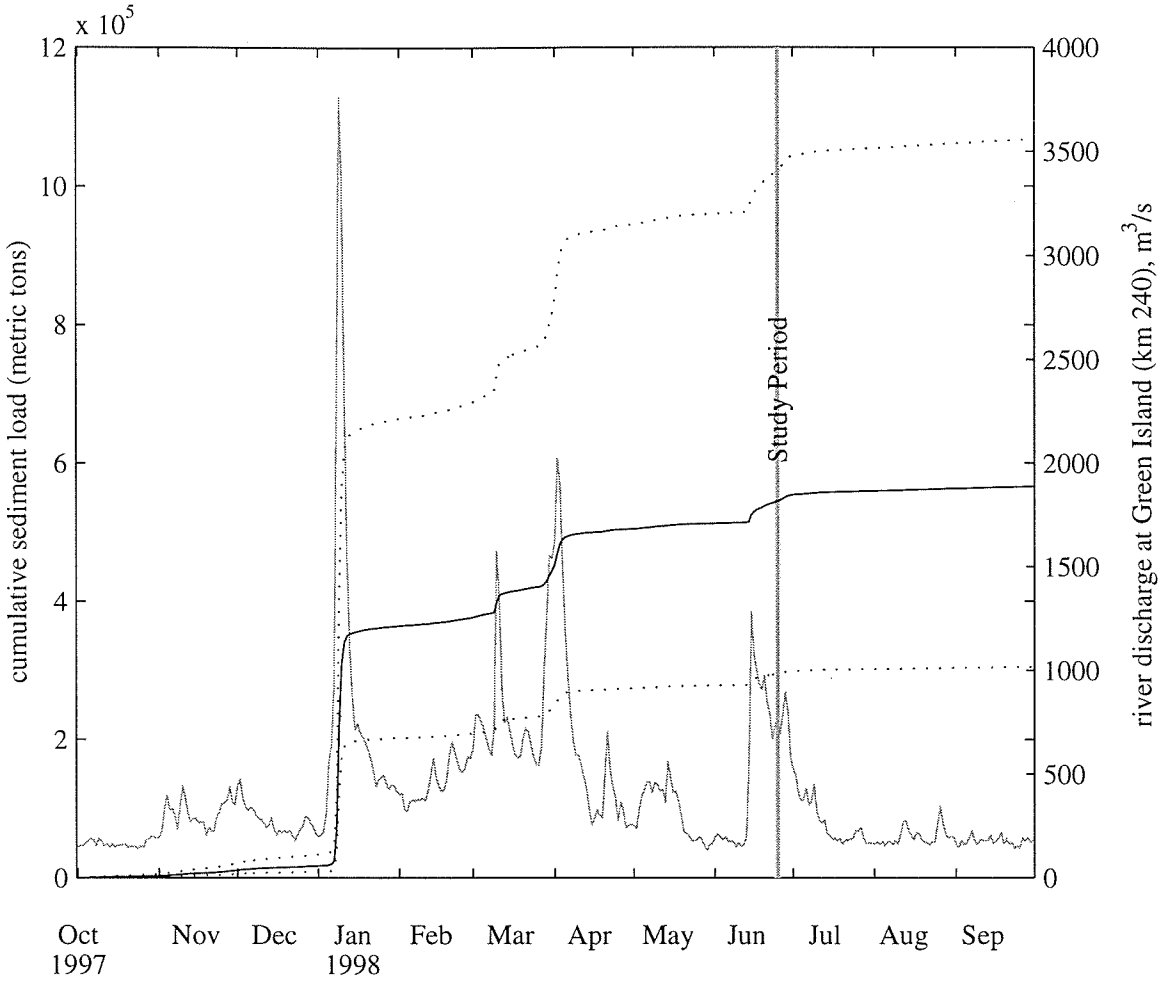

Figure 18: Hudson River discharge and cumulative sediment load past Green Island (km 240) during 1997-1998 water year. Discharge is plotted as a solid line and cumulative sediment load is plotted as a solid black line. The dotted lines represent conservative error estimates for the predicted load.

new deposit was 42 cm for core S-9 and 25 cm for core S-11. The x-radiographs for these cores reveal that new sediment contains fine-scale sedimentary structures of clayey silt strata (0.2 to 3.5 cm thick), separated by thinner laminations of sandy silt (0.05 to 0.2 cm thick). Between 50 and 80 sandy silt laminations were observed within the new sediment of these two cores. In both cores, coarse laminations often appeared in beds separated by 1 to 4 cm thick layers of fine, homogeneous clayey silt. Roughly 17 to 27 couplets of fine/course beds were observed in both core S-11 and S-9.

The large number of laminae found in cores from the southern deposit and the relative dominance of tidal currents in the Lower Hudson River estuary suggest that the observed fine laminae are deposited at the tidal frequency. The formation of the sandy lamination may be similar to the processes identified by Huang and Wang [1987] and Nio and Yang [1991] for the formation of tidal rythmites within sediment of the Changjiang Estuary. The observed sandy laminations in the Hudson could be produced by the high flows associated with peak flood and ebb tides. The raining out of suspended sediment during slack water between flood and ebb may explain the thinner lamination of fine material which separate these coarser laminations. It is difficult, however, to explain how the thick mud beds observed in core S-11 and S-9 could be produced solely by the settling of water column sediment during slack tide. Peak sediment loads over the flood-ebb cycle in the ETM of the Hudson vary between 60 and 500 mg/cm^2 [Geyer, 1995]. Based on these sediment loads and a

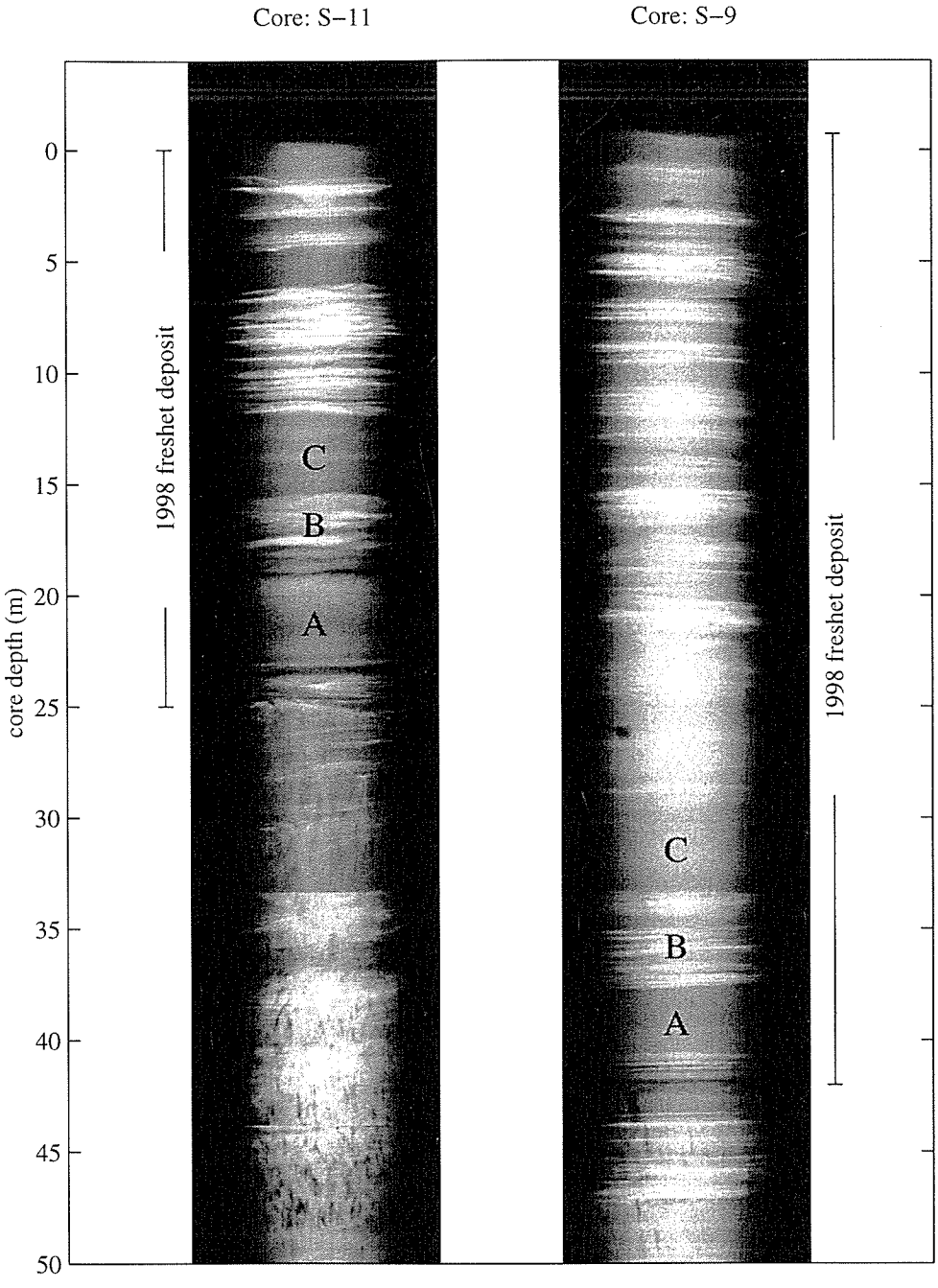

Figure 19: X-radiograph negatives of core S-11 and core S-9. A, B and C labels indicate similar patterns in both cores.

bottom bulk density of 650 kg/m^3 [Panuzio, 1965], the settling of sediment from the water column during slack water in the ETM would only produce a 0.09 to 0.7 cm thick layer of sediment. Mud beds observed in the southern deposit often reached a thickness of 4 cm and are unlikely to be produced solely by this settling process. A comparison with hydrodynamic model studies (discussed in Section 4.1) suggest that the horizontal trapping of sediment may explain the thick mud layers.

Sediment structures observed in the 1998 spring deposit for some cores appear to be spatially correlated. The stratigraphy observed at the bottom of the spring deposit in core S-9 and core S-11 are similar (Figure 19). Both contain two, 4 cm thick homogeneous, fine grained deposits (labeled as A and C in Figure 19) separated by a 4 cm band containing coarser laminations (labeled as B in Figure 19). This correlation seems to show that the sediment accumulation rates between these cores during 1998 were similar for the first 12 cm of deposition. Above this point the spacings between coarse grained laminae are larger in core S-9 than core S-11, possibly reflecting different accumulation rates.

Erosional events may remove fine-scale depositional structures. It is difficult, therefore, to identify the exact age of the observed new sediment solely by the number of fine-scale strata. The number of sandy silt strata observed in the new sediment of S-9 and S-11, however, suggests that this sediment was deposited in no less than 20 days.

4 Discussion

4.1 Comparison with Model Predictions

Figure 20 displays the distribution of the 1998 spring deposit along with the sediment distribution predicted by Geyer et al. [1998]. Both the 1998 observations and model predictions identified a distinct maximum of sediment deposition occurring on the west side of the channel between km 13 and km 15. At this location Geyer [1995] also observed the formation of a salinity front during ebb tide and a strong near-bottom convergence of flow. The correlation between the 1998 observations and model predictions, as well as the water column observations of Geyer [1995], support the hypothesis that sediment is primarily trapped in the southern deposit by a convergence of bottom water flow during ebb tide. Based on the length of the maximum observed within the southern deposit the length scale of this frontal convergence is approximately 2 km.

The focusing of sediment deposition by a convergence of flow may also explain the size of the larger mud layers observed in core S-9 and S-11 (Figure 19). The thickness of such layers are difficult to explain solely by the settling of sediment during slack tide. The focusing of suspended sediment into the convergence zone during ebb tide could dramatically increase deposition within this area, and may result in the formation of the larger mud layers observed in core S-9 and S-11. Why these mud layers are thicker in core S-9 may be due to the spatial structure of the salinity front

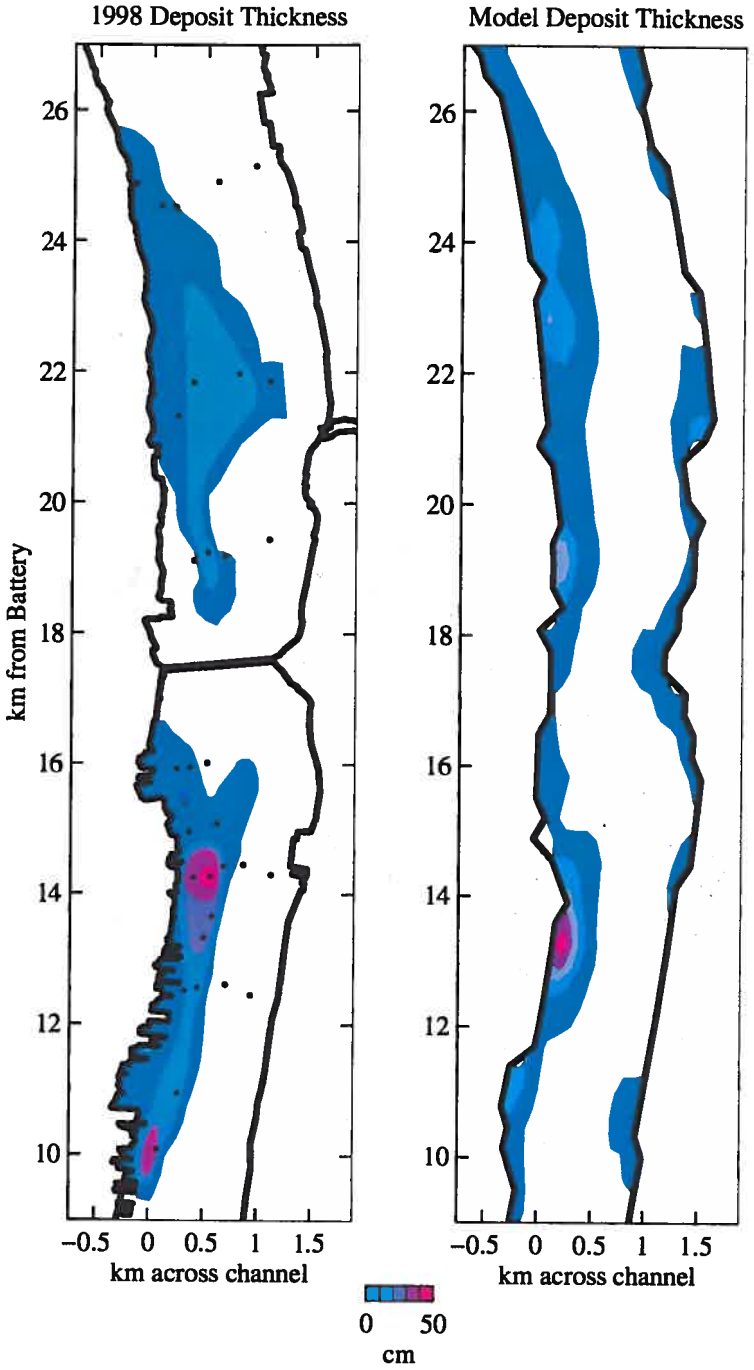

Figure 20: 1998 observations compared to the numerical modeling predictions of Geyer et al. [1997]. The black dots in the figure represent 1998 sampling locations. White areas in the figure represent erosional areas.

that forms within the convergence zone. The formation of this front directly over core S-9 could cause a higher convergence of near-bottom flow at core site S-9 than at core site S-11. During these periods deposition would be higher over S-9 resulting in thicker mud deposits.

The sediment distribution observed north of the George Washington Bridge did not correlate as well with the model predictions of Geyer et al. [1998] (Figure 20). Although sediment was deposited primarily on the west side of the channel in both the model and the 1998 deposit, the observed sedimentation was focused between km 21 and 22, just upstream from the Harlem River. The Harlem River was not incorporated into the model. The abrupt change in deposition near the Harlem River suggests that the river may play a significant role in the structure of sediment deposition in the Lower Hudson River estuary.

It is interesting to note that the northern deposit is approximately the same length as the southern deposit, and located approximately one tidal excursion (10 km) north. A possible explanation is that the northern deposit results from the resuspension, transport and deposition of sediment originally deposited at the southern deposit.

Another point of interest is the limited sediment deposition observed within the vicinity of the George Washington Bridge. The estuary constricts to its minimum cross-sectional area at this point, resulting in increased mixing and higher flows [Panuzio, 1965]. Large bottom shear stresses associated with these high flows could prevent sediment deposition, and may explain the marked coarsening of bottom sed-

iment observed within the vicinity of the bridge.

4.2 Temporal Effects on Deposition

Work by Panuzio [1965], Olsen [1979] and Coch [1986] show that sediment deposited within the Lower Hudson River estuary is primarily river-borne. Results from this study along with work by Panuzio [1965] and Olsen [1979] show that this river-borne sediment is supplied to the estuary primarily during high river discharge events. The high Be-7 activities measured in the new sediment of core S-11 suggest that deposition within the ETM deposits of the Hudson does not occur during these major, high river discharge events, but rather after the spring freshet during normal to low river discharges. Based on the activities of Be-7 and Th-234 on suspended sediment from the Hudson, Feng et al. [1999] found that during low discharge months, sediment is transported into the ETM of the Hudson from more saline sources downstream. High fresh water flows have been found to push the turbidity maximum of an estuary closer to the mouth, resulting in the trapping of sediment further downstream than the usual ETM location [Allen et al., 1980]. After river discharges have relaxed to normal levels this sediment is resuspended and transported back upstream by flood-dominated bottom waters into the usual ETM location. Results from this study are consistent with this variability in estuarine sediment transport. Specifically, sediment deposited in the ETM deposits of the Hudson is transported from downstream sources during periods of normal to low fresh water flow, following high river discharge events

in the spring.

How the spring-neap cycle affects deposition within the Hudson River estuary is not entirely clear. The increase in tidal energy from neap to spring tide causes the Hudson River estuary to transition from strongly stratified to well mixed conditions [Geyer et al., In Press]. The higher flows and reduced frontal behavior during spring tides also results in increased erosion and more widespread resuspension in the estuary [Geyer, 1995]. At the mouth of the Amazon River, the reduction in stratification as tidal amplitude increases from neap to spring results in the thinning of mud bed deposits [Jaeger and Nittrouer, 1995] . At maximum spring tides these mud beds are partially eroded as a result of high flows and weak stratification. A vertical sequence of thinning then thickening of fine/coarse band couplets are observed in both core S-9 and core S-11 and could be the result of a neap-spring process similar to that observed at the mouth of the Amazon.

Based on results from Olsen et al. [1978] it is estimated that approximately 10 to 30 cm/yr of sediment is deposited within the shoaling regions of Lower Hudson River estuary annually. The spring-time accumulations observed in this study match these sedimentation rates. It is not certain how much of the spring deposit is preserved during the rest of the year. Based on dredging records as much as 330,000 metric tons of sediment is deposited annually below the ETM of the Hudson. This suggests that a majority of the new sediment within the southern deposit is preserved until it is removed by dredging. Dredging is not required over the northern deposit, which may

indicate that channel shoaling over this area is minimal. This suggests that the new sediment observed within the northern deposit is not preserved but rather eroded, either during the later part of the year or episodically by large storm events. More work is required, however, to determine the long-term fate of the new spring sediment identified within the ETM deposits.

5 Summary

Geophysical and sedimentological data collected from the Lower Hudson River estuary following the 1998 spring freshet show that:

- There is a high degree of spatial and temporal variability in sedimentation within the estuary.

- An estimated 300,000 metric tons of sediment was deposited below the ETM of the estuary between May and June of 1998. This inventory can accounts for 30 to 98 percent of the annual fluvial sediment load supplied to the estuary during the 1997-1998 water year.

- Two primary deposits exist within the ETM for the estuary and the locations of these deposits are consistent with the trapping mechanisms identified by Geyer [1995] and Geyer et al. [1998].

- The spatial distribution of new sediment within the ETM deposits along with the fine-scale stratigraphy within this sediment support the theory that sediment is primarily trapped below the ETM by a convergence of flow, due to the formation of a longitudinal salinity front during ebb tide.

References

K. A. Abood. Circulation in the hudson estuary. *Annals of the New York Academy of Sciences*, 250:39–111, 1974.

NY District ACOE. Dredged material management plan for the port of new york and new jersey., Sep 1996. Interim Report.

G. P. Allen and H. W. Postmentier. Sequence stratigraphy and facies model of an incised valley fill: The gironde estuary, france. *Journal of Sedimentary Geology*, 63:378–391, 1993.

G. P. Allen, J. C. Salmon, P. Bassoullet, Y. Du Penhoat, and C. De Grandpre. Effects of tides on mixing and suspended sediment transport in macrotidal estuaries. *Sedimentary Geology*, 26:69–90, 1980.

R. B. Biggs. The sediments of the chesapeake. In G. H. Luaff, editor, *Estuaries*, pages 239–260. Amer. Assoc. Adv. Sci., Washington, DC, 1967.

M.H. Bothner, P.W. Gill, W.S. Boothman, B.B. Taylor, and H.A Karl. Chemical and textural characteristics of sediments at an epa reference site for dredged material on the continental slope sw of the farallon islands. Open-File Report 97-87, U.S. Geological Survey, Woods Hole Field Center, 1997.

P. C. Chatwin. Some remarks on the maintenance of the salinity distribution in estuaries. *Estuarine and Coastal Marine Science*, 4:555–566, 1976.

N. K. Coch. Sediment characteristics and facies distributions in the hudson system. *Northeastern Geology*, 8:109–129, 1986.

William Danforth. *Xsonar/Showimage: A complete system for rapid sidescan sonar processing and display.* U.S. Geological Survey, Woods Hole Field Center, Quissett Campus, Woods Hole, MA. 02543, 1997. Open-File Report 97-686.

T. K. Edwards and G. D. Glysson. *Field methods for measurement of fluvial sediment.* U.S. Geological Survey, 1988. Open-File Report 86-531.

H. Feng, J. K. Cochran, and Hirschberg D. J. Th-234 and be-7 as tracers for the sources of particles to the turbidity maximum of the hudson river estuary. *Estuarine, Coastal and Shelf Science*, 1999.

H. Feng, K. J. Cochran, D. J. Hirschberg, and R. E. Wilson. Small-scale spatial variations on natural radionuclide and trace metal distributions in the sediment from the hudson river estuary. *Estuaries*, 21:263–280, 1998.

R. D. Flood and H. J. Bokuniewicz. Bottom morphology in the hudson river estuary and new york harbor. *Northeastern Geology*, 8:130–140, 1986.

Robert L. Folk. *Petrology of sedimentary rocks*, chapter 3. Hemphill Oublishing Company, 1980.

W. R. Geyer. The importance of suppression of turbulence by stratification on the estuarine turbidity maximum. *Estuaries*, 16:113–125, 1993.

W. R. Geyer. Final report: Particle trapping in the lower hudson estuary. Submitted to Hudson River Foundation, April 1995.

W. R. Geyer, Trowbridge J., and M. Bowen. The dynamics of a partialy mixed estuary. *Journal of Physical Oceanograph*, In Press.

W. R. Geyer, R. P. Signell, and G. C. Kineke. Lateral trapping of sediment in a partially mixed estuary. In *Proc. of the 8th International Biennial Conference on Physics of Estuaries and Coastal Seas*, 1998.

R. J. Gibbs, L. Tshudy, D. M. andKonwar, and J. M. Martin. Coagulation and transport of sediment in the gironde estuary. *Sedimentology*, 36:987–999, 1989.

M. G. Gross. Sediment and waste deposition in the new york harbor. *Annals New York Acad. Sci.*, 250:112–128, 1974.

D. J. Hirschberg and H. J. Bokuniewicz. Measurements of water, temperature, salinity and suspended sediment concentrations along the axis of the hudson river estuary 1980-1981. Special Data Report: Marine Sciences Research Center, State University of New York, 1991. Report 11, Reference 91-14.

D. J. Hirschberg, P. Chin, H. Feng, and J. K. Cochran. Dynamics of sediment and contaminant transport in the hudson river estuary: evidence from sediment distributions of naturally occurring radionuclides. *Estuaries*, 19:931–949, 1996.

S. Huan-ting, Z. Hui-fang, and M. Zhi-chang. Circulation of the chang jiang estuary and its effect on the transport of sediment. In V.S. Kennedy, editor, *Estuarine Comparisons*, pages 677–676. Academic Press, New York, 1982.

N. Huang and G. Wang. The new criteria of ancient tidal sediments-tidal cycle sequence. *Acta Sedimentologica Sinica*, 5:39–44, 1987.

J. M. Jaeger and C. A. Nittrouer. Tidal controls on the formation of fine-scale sedimentary strata near the amazon river mouth. *Marine Geology*, 125:259–281, 1995.

H. J. Knebel, R. R. Rendigs, and Bothner M. H. Modern sedimentary environments in boston harbor, massachusetts. *Journal of Sedimentary Petrology*, 61:791–804, 1991.

L. R. LeBlanc, L. Mayer, M. Rufino, S. G. Schock, and J King. Marine sediment classification using chirp sonar. *J. Acoust. Soc. Am.*, 91:107–115, 1992.

W. Lick and H. Huang. Flocculation and the physical properties of flocs. In A. J. Mehta, editor, *Nearshore and Estuarine Cohesive Sediment Transport*, pages 21–39. American Geophysical Union, Washington, DC, 1993.

E. R. Long, D. A. Wolfe, J. K. Scott, G. B. Thursby, E. A. Stern, C. Peven, and T. Schwartz. Magnitude and extent of sediment toxicity in the hudson-raritan estuary., 1995. NOAA Technical Memorandum NOS ORCA 88.

D. B. Nash. Effective sediment-transporting discharge from magnitude-frequency analysis. *The Journal of Geology*, 1994:79–95, 1991.

M. Nichols and G. Poor. Sediment transport in a coastal plain estuary. *Proceeds of the American Society of Civil Engineers*, 93:83–95, 1967.

M. M. Nichols, G. H. Johnson, and P. C. Peebles. Modern sediments and facies model for a microtidal coastal plain estuary, the james estuary, virginia. *Journal of Sedimentary Petrology*, 61:883–899, 1991.

S. D. Nio and C. Yang. Diagnostic attributes of clastic tidal deposits; a review. In *Clastic Tidal Sedimentology*. Canadian Society of Petroleum Geologists, 1991.

C. B. Olsen. *Radionuclides, sedimentation and the accumulation of pollutants in the Hudson Estuary*. PhD thesis, Columbia University, 1979.

C. B. Olsen, I. L. Larsen, P. D. Lowry, N. H. Cutshall, and M. M. Nichols. Geochemistry and deposition of be-7 in river-estuarine and coastal waters. *Journal of Geophysical Research*, 91:896–908, 1986.

C. B. Olsen, H. J. Simpson, R. F. Bopp, S. C. Williams, T. H. Peng, and B. L. Deck. A geochemical analysis of the sediments and sedimentation in the hudson estuary. *Journal of Sedimentary Petrology*, 48:401–418, 1978.

F. L. Panuzio. Lower hudson river siltation. In *Proc. of the Ferral InterAgency Sedimentation Conference*, pages 512–550. Agriculture Research Service, 1965. Misc. Pub. 970.

H. Postma. Sediment transport and sedimentation in the estuarine environment. In G. H. Lauff, editor, *Estuaries*, pages 158–179. American Association for the Advancement of Science, Washington, D.C., 1967.

W. B. Ryan and R. D. Flood. Side-looking sonar backscatter response at dual frequencies. *Marine Geophysical Researches*, 18:689–705, 1996.

K. S. Squibb, J.M. O'Connor, and T. J. Kneip. Ny/nj harbor estuary program. module 3.1: Toxics characterization report, 1991. NYD/USEPA Region 2.

L. M. J. U. Van Straaten. Composition and structure of recent marine sediments in the netherlands. *Leidse Geol. Mededel.*, 19:1–110, 1954.

L. D. Wright, D. B. Prior, C. H. Hobbs, R. J. Byrne, J. D. Boon, L. C. Schaffner, and M. O. Green. Spatial variablility of bottom types in the lower chesapeake bay and adjoining estuaries and inner shelf. *Estuarine, Coastal and Shelf Science*, 24: 765–784, 1987.